

1 Dynamics of Variable Dusk-Dawn Flow Associated with Magnetotail 2 Current Sheet Flapping

3
4 James H. Lane¹, Adrian Grocott¹, Nathan A. Case¹, Maria-Theresia Walach¹

5
6 ¹ Department of Physics, Lancaster University, Lancaster, UK

7
8 Correspondence to: James Lane (j.lane@lancaster.ac.uk)

9 10 11 Abstract

12 Previous observations have provided a clear indication that the dusk-dawn ($v_{\perp y}$) sense of
13 both slow ($< 200 \text{ km s}^{-1}$) and fast ($> 200 \text{ km s}^{-1}$) convective magnetotail flows is strongly
14 governed by the Interplanetary Magnetic Field (IMF) B_y conditions. The related ‘untwisting
15 hypothesis’ of magnetotail dynamics is commonly invoked to explain this dependence, in
16 terms of a large-scale magnetospheric asymmetry. In the current study, we present Cluster
17 spacecraft observations from 12 October 2006 of earthward convective magnetotail plasma
18 flows whose dusk-dawn sense disagrees with the untwisting hypothesis of IMF B_y control of
19 the magnetotail flows. During this interval, observations of the upstream solar wind
20 conditions from OMNI, and ionospheric convection data using SuperDARN, indicate a large-
21 scale magnetospheric morphology consistent with positive IMF B_y penetration into the
22 magnetotail. Inspection of the in-situ Cluster magnetic field data reveals a flapping of the
23 magnetotail current sheet; a phenomenon known to influence dusk-dawn flow. Results
24 from the curlometer analysis technique suggest that the dusk-dawn sense of the $\mathbf{J} \times \mathbf{B}$ force
25 was consistent with localised kinks in the magnetic field and the flapping associated with
26 the transient perturbations to the dusk-dawn flow observed by the Cluster 1 spacecraft. We
27 suggest that the IMF B_y penetration at the location of Cluster was unable to override the
28 variable dusk-dawn flow associated with the flapping. We conclude that invocation of the
29 untwisting hypothesis may be inappropriate when interpreting intervals of dynamic
30 magnetotail behaviour such as during current sheet flapping, particularly at locations where
31 magnetotail flaring becomes dominant.

32

33 **1. Introduction**

34

35 Convective magnetotail plasma flows at Earth, driven by the closing of magnetic flux via
36 reconnection as part of the Dungey Cycle (Dungey, 1961) have been studied extensively for
37 many years (e.g. Angelopoulos et al. 1992, 1994; Sergeev et al., 1996; Petrukovich et al.,
38 2001; Cao et al., 2006; McPherron et al., 2011; Frühauff & Glassmeier, 2016). Arguably, the
39 most well studied of these is the Bursty Bulk Flow (BBF). Angelopoulos et al. (1994) defined
40 BBFs as being channels of earthward plasma flow continually above 100 km s^{-1} , exceeding
41 400 km s^{-1} at one point across some interval, usually across a timescale of a few minutes.
42 The flows are said to be the main transporter of mass, energy and flux in the magnetotail
43 (e.g. Angelopoulos et al., 1994; Nakamura et al., 2002; Grocott et al., 2004a; Kiehas et al.,
44 2018). Although their earthward nature is the key defining characteristic of BBFs, they will
45 invariably exhibit a dusk-dawn component in their bulk flow as well (e.g. Angelopoulos et
46 al., 1994; Petrukovich et al., 2001; Grocott et al., 2004b). Understanding the drivers of dusk-
47 dawn asymmetries in magnetospheric dynamics is an important element of geospace
48 research (e.g. Haaland et al., 2017).

49

50 Magnetotail flows are generally expected to be symmetric about midnight, at least in the
51 absence of any asymmetry (e.g. Kissinger et al., 2012). A key factor that has been observed
52 to influence the dusk-dawn direction of the magnetotail flow, however, is the B_y component
53 of the Interplanetary Magnetic Field (IMF). It is well established that when the IMF
54 reconnects with the dayside terrestrial magnetic field, a non-zero IMF B_y component leads
55 to asymmetric loading of open flux into the polar cap (e.g. Khurana et al., 1996; Tenfjord et
56 al., 2015; Grocott et al., 2017; Ohma et al., 2019). This results in a twisting of the
57 magnetotail whereby the closed field lines are rotated about the midnight meridian, and a
58 B_y component is superimposed onto the tail field as a consequence of IMF B_y penetration
59 (Cowley, 1981; Petrukovich, 2011; Tenfjord et al., 2015). Subsequently, following nightside
60 reconnection, the tail will untwist (Grocott et al., 2004c), with the excitation of multiple
61 convective flow bursts, each with an earthward and dusk-dawn component, in the tail and
62 nightside ionosphere (Grocott et al., 2007). In order to be consistent with the tail
63 'untwisting hypothesis', any convective flows associated with an individual tail field line

64 should share the same dusk-dawn direction (e.g. see Figure 3 of Grocott et al., 2005). The
65 role of IMF B_y in the untwisting hypothesis has been examined previously in a number of
66 studies (e.g. Grocott et al., 2007; Pitkänen et al., 2013, 2015, 2017). These studies revealed
67 that under prolonged positive IMF B_y conditions, the earthward flows are expected to
68 exhibit a dawnward component in the northern hemisphere ($B_x > 0$) and a duskward
69 component in the southern hemisphere ($B_x < 0$), with the opposite correlation for negative
70 IMF B_y conditions. This is especially true close to midnight, where the penetration of IMF B_y
71 is particularly noticeable. Further away from midnight, however, effects such as magnetotail
72 flaring (Fairfield, 1979) are expected to produce a dominant B_y component, which may
73 suppress IMF B_y -effects on the dusk-dawn asymmetry, resulting in the symmetric earthward
74 convection of field lines (e.g. see Fig. 2 of Pitkänen et al., 2019). Nevertheless, IMF B_y has
75 been shown to govern the dusk-dawn nature of these flows both during periods of steadier,
76 slower convection (Pitkänen et al., 2019), as well as during more transient, dynamic BBF-like
77 intervals (Grocott et al., 2007) at up to $7 R_E$ towards the dusk-dawn flanks (Pitkänen et al.,
78 2013). In the present study, we present Cluster observations of dawnward and duskward
79 directed flows that do not match this expected dependence on IMF B_y , implying that the
80 untwisting hypothesis is insufficient in this case. In particular, we highlight the problematic
81 nature of the observation of dawnward flow, in relation to the pre-midnight location of
82 Cluster. We instead suggest that the flows are being driven by local perturbations due to
83 dynamic behaviour of the tail that are associated with flapping of the current sheet.

84

85 The current sheet, or 'neutral' sheet, lies in the equatorial plane at the center of the tail
86 plasma sheet and separates the earthward ($B_x > 0$) and tailward ($B_x < 0$) directed field (Ness,
87 1965). The current sheet is a highly dynamic region of the Earth's magnetotail which can
88 undergo various types of net motion, such as tilting due to lobe magnetic pressures (Cowley
89 et al., 1981; Tenfjord et al., 2017) as well as flapping. Flapping of the current sheet can
90 generally be described as a sinusoidal-like variation in B_x of up to tens of nanoTesla, where
91 an observing spacecraft often measures repeated changes in the sign of B_x (e.g. Runov et al.,
92 2009), indicative of crossings of the current sheet, with characteristic times ranging from a
93 few seconds to (more commonly) several minutes (e.g. Runov et al., 2009; Wu et al., 2016;
94 Wei et al., 2019). Drivers of current sheet flapping have been widely investigated, with
95 possible causes ranging from external solar wind/IMF changes (Runov et al., 2009),

96 induction of hemispheric plasma asymmetries (Malova et al., 2007; Wei et al., 2015), fast
97 earthward flow (Nakamura et al., 2009) as well as periodical, unsteady magnetotail
98 reconnection (Wei et al., 2019). Studies such as Volwerk et al. (2008) and Kubyshkina et al.
99 (2014) have illustrated that flapping of the current sheet can be associated with variable
100 dusk-dawn flow, potentially overriding, or preventing any IMF B_y control of the flow.

101

102 In this paper we present Cluster spacecraft observations of an interval of dynamic
103 magnetotail behaviour on 12 October 2006. Throughout this interval, Cluster 1 observed
104 oscillations in the magnetic field B_x component, which we attribute to current sheet
105 flapping, concurrent with a series of convective fast flows with significant and variable dusk-
106 dawn components. The B_y component of the concurrent upstream IMF had been largely
107 positive for several hours prior to the flapping. Consequently, the interval discussed here
108 provides an opportunity to investigate the possible competition of two distinct mechanisms
109 for control of the dusk-dawn flow: 1) IMF B_y and 2) localized dynamics related to the
110 flapping of the current sheet. In contrast to studies which have come before such as those
111 presented by Grocott et al. (2007) and Pitkänen et al. (2015), the observed dusk-dawn
112 direction of transient flow enhancements in this case disagrees with that which might be
113 expected from the prevailing IMF B_y conditions, despite clear evidence for global
114 penetration of positive IMF B_y . We therefore suggest that IMF B_y penetration at the location
115 of Cluster was unable to overcome the variable dusk-dawn flow associated with the
116 flapping.

117

118 **2. Instrumentation and Data Sets**

119 *2.1. Spacecraft Data*

120 The magnetospheric observations presented in this case study were made by the Cluster
121 multi-spacecraft (C1-C4) constellation (Escoubet et al., 2001). We make use of the fluxgate
122 magnetometer (FGM) onboard the Cluster spacecraft to obtain magnetic field
123 measurements (Balogh et al., 2001), and obtain our bulk ion velocity data from the Hot Ion
124 Analyser (HIA) on C1 and C3 calculated as on-board moments (Rème et al., 1997). The
125 magnetic field data presented are 5 vectors-per-second (0.2s res) which have been 1s
126 median-averaged, with the velocity data presented having spin resolution of just over 4s.
127 Where these datasets have been combined to produce parameters such as the plasma beta

128 and field-perpendicular velocities, we have resampled both the magnetic field and plasma
 129 data to 5s resolution. All data are presented in geocentric solar magnetospheric (GSM)
 130 coordinates unless stated otherwise.

131

132 The interval of study in this paper occurred between 00:00 – 00:55 UT on 12 October 2006.

133 At 00:00 UT the Cluster spacecraft were located in the near-Earth magnetotail plasma sheet,

134 in the pre-midnight sector. C1 was located at $(X = -14.7, Y = 6.0, Z = -1.2)$ R_E , C2 at $(X =$

135 $-14.2, Y = 7.5, Z = -0.7)$ R_E , C3 at $(X = -13.9, Y = 7.0, Z = -2.1)$ R_E , and C4 at $(X = -13.2, Y = 6.2,$

136 $Z = -0.8)$ R_E . This is depicted in Fig. 1a by the colored triangles, along with the respective

137 spacecraft trajectories, from 00:00 – 00:55 UT, by the solid lines. Fig. 1b shows a zoomed-

138 out version of Fig. 1a, which illustrates the location of the spacecraft with respect to the

139 Earth. Fig. 1b also shows a traced modelled magnetic field line, achieved using the semi-

140 empirical TA15 model of the magnetosphere (Tsyganenko & Andreeva, 2015), which passes

141 through the location of C1 and connects to both the northern and southern hemispheres of

142 the Earth. We parameterised the TA15 model using mean-averaged solar wind dynamic

143 pressure (P_{dyn}), IMF B_y and IMF B_z data from the 1-hour interval prior to 00:28 UT (the start

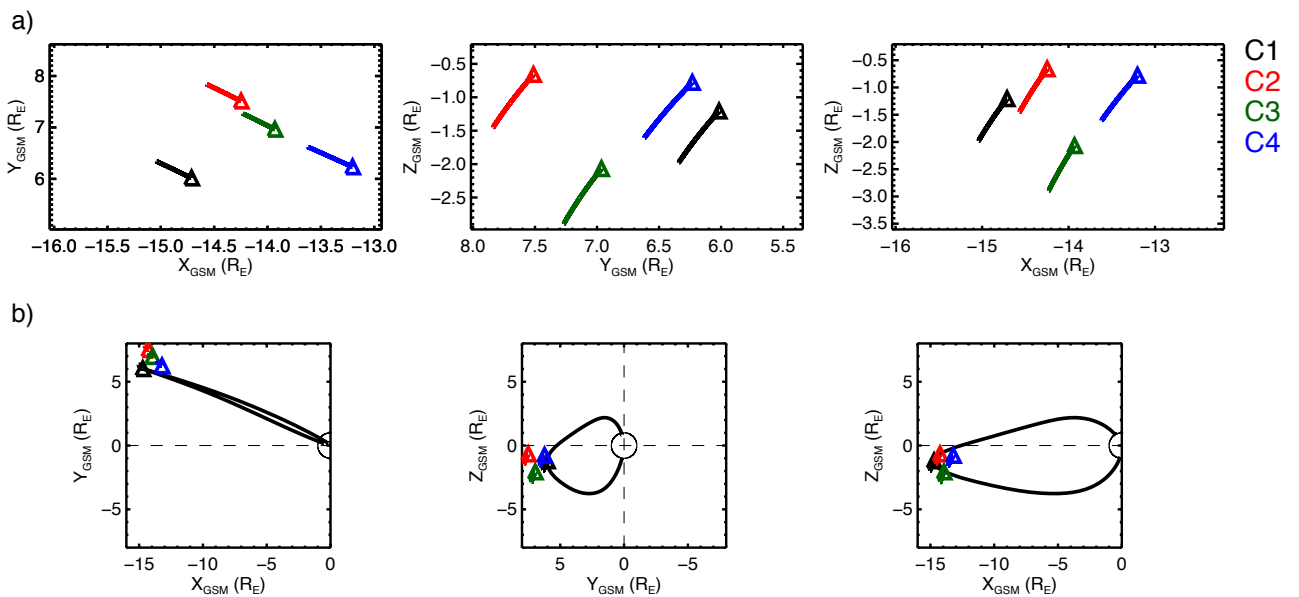
144 of our specific interval of interest). These values were $P_{dyn} = 1.56$ nPa, IMF $B_y = +1.56$ nT and

145 IMF $B_z = -2.17$ nT. There was also a tailward dipole tilt of $\approx -12^\circ$. The model was also

146 parameterised with a solar wind coupling function index known as the ‘N index’, after

147 Newell et al. (2007). The N index varies between 0 (quiet) and 2 (very active), and in this

148 instance was ~ 0.4 .



149

150 **Figure 1:** a) The locations of the Cluster spacecraft in the X-Y, Y-Z, and X-Z GSM planes, from
151 left to right, respectively, at 00:00 UT on 12 October 2006, marked by the triangles. The
152 trajectories from 00:00 UT to 00:55 UT are marked by the solid lines. The spacecraft are
153 color-coded according to the key on the right. b) As in a), with a zoomed-out view. The Earth
154 is shown by the solid circle. A TA15 model magnetic field line passing through the location of
155 C1 is shown as the solid black line.

156

157 The IMF measurements used in this study were provided by the OMNIweb database at 1-
158 minute resolution, having been first propagated from L1 to the bow shock nose (King &
159 Papitashvili, 2005).

160

161 *2.2. SuperDARN Data*

162 The ionospheric observations presented in section 3.3 were provided by the Super Dual
163 Auroral Radar Network (SuperDARN), an international collaboration of 36 ground-based
164 radars (Nishitani et al., 2019) that make line-of-sight Doppler measurements of the
165 horizontal motion of the ionospheric plasma every few seconds (e.g. Chisham et al., 2007).
166 Here, we use 2-min ionospheric convection maps created by fitting the line-of-sight $\mathbf{E} \times \mathbf{B}$
167 velocity data to an eighth order expansion of the ionospheric electric potential in spherical
168 harmonics using the technique of Ruohoniemi & Baker (1998), implemented in the Radar
169 Software Toolkit (RST version 4.2, 2018). To accommodate intervals with limited data
170 availability, the data are supplemented with values derived from a statistical model
171 parameterized by IMF conditions. This is a well-established technique that has been
172 thoroughly discussed by, e.g., Chisham et al. (2007). The convection maps we present
173 employ the commonly used model of Ruohoniemi & Greenwald (1996). As a check on the
174 sensitivity of the maps to the choice of model input, we also tested the fitting using the
175 alternative model of Thomas and Shepherd (2018) and found that this has little impact on
176 the maps and no impact on our conclusions.

177

178 As a further measure to ensure that the choice of model is not critical to our results, we
179 chose not to use the concurrent IMF vector to parameterise the background model. In this
180 case, because we are using the SuperDARN data to provide evidence in support of the
181 expected large-scale influence of IMF B_y , we deemed it inappropriate to include model data

182 already parametrised by IMF B_y . We instead specify a nominal southward IMF with zero B_y
183 component in our analysis, to ensure that a background model with no pre-existing IMF B_y
184 influence is used. Although this might result in the patterns we show being less accurate
185 overall, especially in regions of poor data coverage, it will ensure that any B_y -associated
186 asymmetry in the maps is driven by the radar data from our interval of study, and not the
187 background model. This is discussed further in section 4.1, below.

188

189 **3 Observations**

190

191 In this section we present observations of the IMF, magnetotail magnetic field and plasma
192 flow, and ionospheric convection from an interval on 12 October 2006.

193

194 *3.1 IMF Observations*

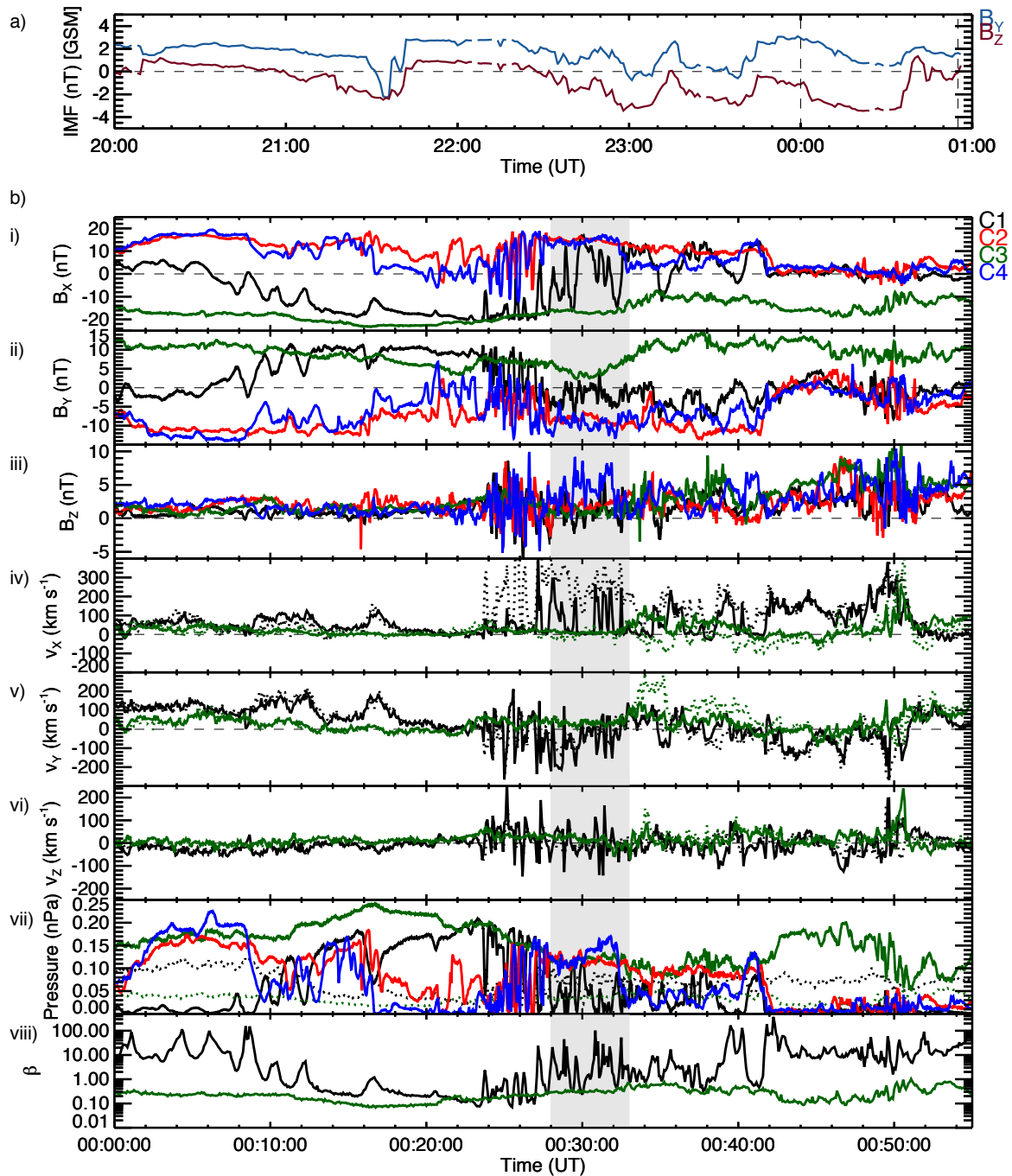
195 Figure 2 presents an overview of the spacecraft data from an extended interval around our
196 period of specific interest for broader context. In Figure 2a, we show a time-series of the
197 IMF B_y and IMF B_z data from 20:00 UT on 11 October to 01:00 UT on 12 October 2006. These
198 data reveal that IMF B_y was generally positive for several hours prior to the fast flow
199 interval, with IMF B_z predominantly negative. There were three small intervals of negative
200 IMF B_y at \sim 21:35 UT, 23:00 UT and 23:40 UT and we discuss the possible ramifications of
201 these, and our treatment of them, in section 4.1.

202

203 *3.2 Cluster Spacecraft Observations*

204 In Figure 2b, we present the in-situ magnetic field and plasma measurements from the
205 Cluster spacecraft across the interval 00:00 – 00:55 UT.

206



207

208 **Figure 2:** a) A plot of the IMF time series data for the IMF B_y (blue) and IMF B_z (red)
 209 components, from 20:00 UT on 11 October 2006 to 01:00 UT on 12 October 2006. The
 210 vertical dashed lines indicate the start (00:00 UT) and end (00:55 UT) of the interval of
 211 Cluster data (below). b) The in-situ Cluster spacecraft measurements. Shown first is the local
 212 magnetic field data, i) B_x , ii) B_y and iii) B_z , followed by the bulk ion velocity data, iv) v_x , v) v_y ,
 213 and vi) v_z (dotted lines). The field-perpendicular component of the ion flow (indicative of
 214 the $\mathbf{E} \times \mathbf{B}$ convection) is shown in panels iv) to vi) by the solid lines. In panel vii) the magnetic

215 $\left(\frac{B^2}{2\mu_0}\right)$ and thermal ion (nkT) pressures are shown by the solid and dotted lines respectively,
 216 and in panel viii) the ion plasma beta from C1 and C3 is shown. All data are labelled
 217 according to the color-coded key on the right-hand side. The time-interval between the gray
 218 shaded region marks our specific interval of interest (discussed in text).

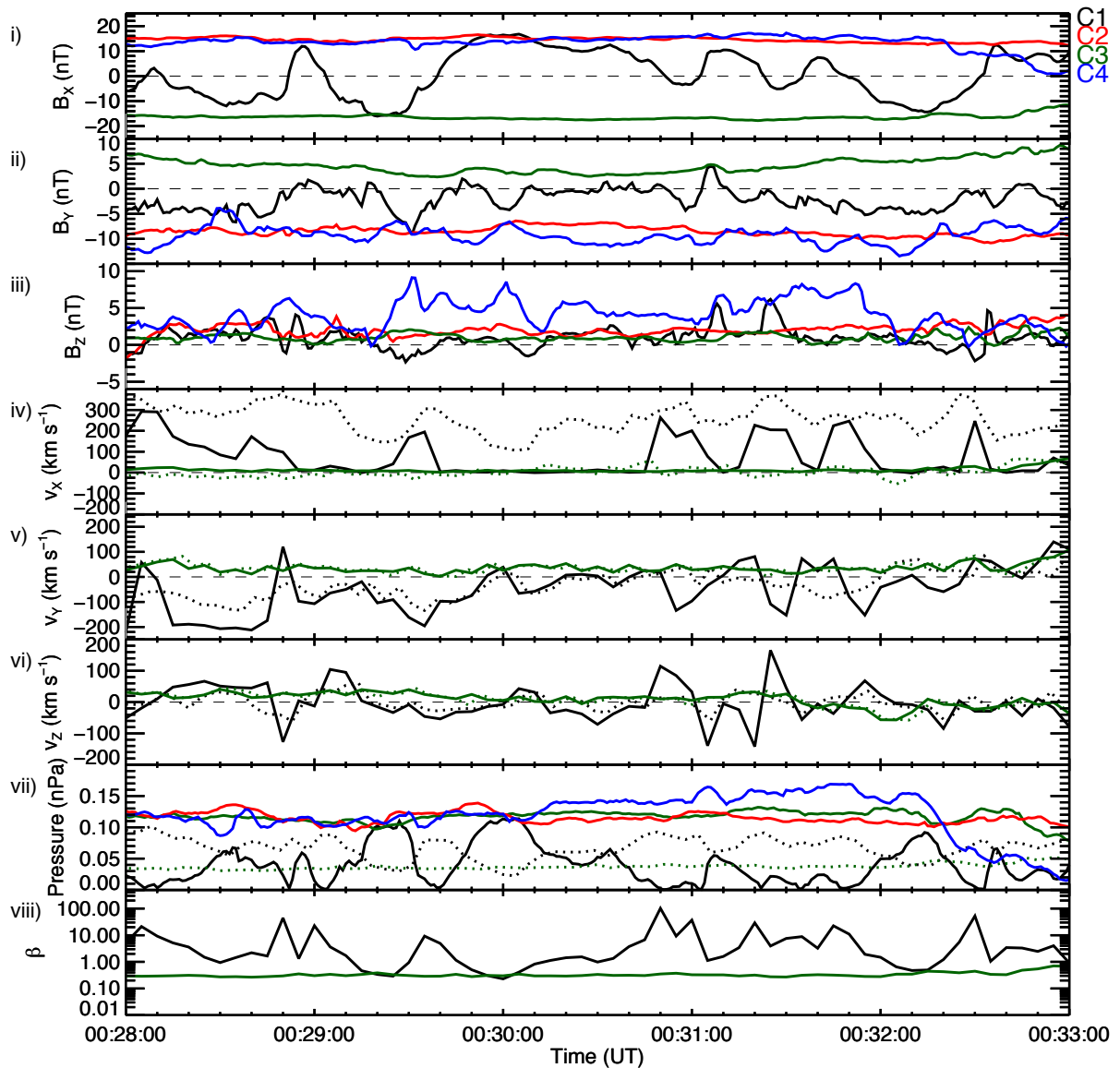
219
 220

221 At $\sim 00:06$ UT, C1 crossed from the northern hemisphere into the southern hemisphere,
 222 illustrated by the sign change in B_x from positive to negative shown in Fig. 2b i). Coincident
 223 with this, the observed B_y , shown in Fig. 2b ii) turned from negative to positive, consistent
 224 with the expected B_y due to magnetotail flaring (see section 4.2) at this pre-midnight
 225 location (Fairfield, 1979). Fig. 2b iv) reveals that up until $\sim 00:24$ UT, the bulk earthward flow
 226 (v_x , dotted lines) and field-perpendicular flow ($v_{\perp x}$, solid lines) measured by both C1 and C3
 227 was generally low in magnitude ($< 100 \text{ km s}^{-1}$). The dusk-dawn (v_y) component of the flow,
 228 shown in Fig. 2b v), remained steadily duskward ($v_y > 0$) at C1 and duskward or close to zero
 229 at C3. The north-south (v_z) component of the flow in Fig. 2b vi), measured by C1 and C3 was
 230 effectively zero. During this period, the Cluster spacecraft that resided in the northern
 231 hemisphere (predominantly C2 and C4), observed $B_y < 0$, and the spacecraft which resided
 232 in the southern hemisphere (predominantly C1 and C3) observed $B_y > 0$, again consistent
 233 with magnetotail flaring. Occasionally a spacecraft encountered the current sheet ($B_x = 0$) at
 234 which point it observed $B_y = 0$. We comment on the significance of these magnetic field
 235 observations in section 4.2.

236

237 After $\sim 00:24$ UT, C1 began to observe a period of enhanced earthward flow
 238 ($v_x > 300 \text{ km s}^{-1}$) and variable dusk-dawn flow, concurrent with sudden variation in the local
 239 B_x component. Similarly, C2 and C4, but not C3, observed large magnitude ($> 20 \text{ nT}$) rapid
 240 variations in B_x , which appear to have an apparent timescale of around a minute and which
 241 we attribute to a flapping of the current sheet. As well as rapid variations in B_x , both the B_y
 242 and B_z components of C1, C2 and C4 seemed highly variable. As perhaps to be expected,
 243 these variations in the magnetic field were accompanied by significant variations in the
 244 magnetic pressure of $\sim 0.15 \text{ nPa}$, as shown by the solid lines in Fig. 2b vii).

245 Unlike the other spacecraft, C3 remained in the southern hemisphere throughout the entire
 246 interval and did not observe the rapid fluctuations in B_x . Between 00:28 – 00:33 UT (the gray
 247 shaded region), C1 began to repeatedly and rapidly cross the current sheet, as previously
 248 experienced by C2 and C4, whilst continually observing enhanced earthward flow and
 249 variable dusk-dawn convective flow ($v_{\perp y}$). Across the entire interval, the plasma beta, β ,
 250 indicated in Fig. 2b viii), measured by C3 remained above ~ 0.1 , with C1's measured β
 251 ranging from 0.1 to over 100. This is consistent with the fact that C1 was continually
 252 crossing the current sheet at the center of the plasma sheet, where β is larger (Baumjohann
 253 et al., 1989). It is this interval of current sheet crossing and variable flow observed by C1
 254 that we focus on below and is presented in more detail in Figure 3.



255

256 **Figure 3:** As in Fig. 2b, but for the interval 00:28 – 00:33 UT on 12 October 2006.

257

258 Fig. 3 i) conveys the extent of the large-amplitude B_x variations observed by C1 between
259 00:28 and 00:33 UT. B_x was generally fluctuating between positive and negative values
260 throughout the five-minute interval, with a minimum at ~ -16 nT and maximum at ~ 17 nT.
261 The magnetic pressure at C1 shown by the solid black line in Fig. 3 vii) is consistent with the
262 idea that C1 was crossing the current sheet, as this generally reached minima at the center
263 of each current sheet crossing ($B_x \approx 0$). The B_y component (Fig. 3ii) measured by C1 generally
264 remained negative and highly variable for the entire interval, with a number of large
265 negative enhancements and a few small positive excursions. It is particularly of note that
266 when C1 was below the neutral sheet, as implied by a negative B_x component, B_y was
267 almost always negative. As we discuss in section 4.2, this is inconsistent with what we would
268 expect based on the location of the spacecraft and also inconsistent with any expectation
269 that a positive IMF B_y should have penetrated into the tail. The B_z component (Fig. 3iii)
270 generally remained positive with some small negative excursions.

271

272 Unlike C1, C2-4 measured generally steady B_x throughout this five-minute period. C2 and C4
273 measured positive B_x , indicating that they were above the neutral sheet, and C3 measured
274 negative B_x , indicating that it was below the neutral sheet. Similarly, B_y was steadily negative
275 for C2 and C4 and steadily positive for C3. Again, we note the inconsistency between the C1
276 and C3 observations of B_y ; when in the southern hemisphere C1 generally observed $B_y < 0$,
277 whereas C3 observed $B_y > 0$. On a few separate occasions C1 did briefly observe $B_y > 0$ (e.g.
278 at 00:31:05 UT) but at these times C1 was located above the neutral sheet ($B_x > 0$), while C2
279 and C4 observed $B_y < 0$ above the neutral sheet. These variations in B_y imply the observation
280 of a 'kink' in the field at the location of C1, the ramifications of which are discussed further
281 in section 4.2.

282

283 At times when B_x observed by C1 was negative, indicating that C1 was below the neutral
284 sheet, C1 generally observed negative (dawnward) $v_{\perp y}$ (Fig. 3v) with a magnitude varying
285 between 100 and 200 km s⁻¹. At times when B_x became positive, indicating that C1 was
286 above the neutral sheet, C1 observed positive (duskward) $v_{\perp y}$ a majority of the time,
287 although this flow barely reached 100 km s⁻¹. The negative enhancements in $v_{\perp y}$ were

288 generally accompanied by negative enhancements in B_y . Across the interval, there was a
289 near continual $v_x > 200 \text{ km s}^{-1}$ flow (black dotted line in Fig. 3iv), peaking at almost 400 km
290 s^{-1} , with concurrent peaks in the convective $v_{\perp x}$ component (solid black line) of at least
291 200 km s^{-1} . The convective flow measured by C3, however, was generally very weak ($|v_{\perp}| <$
292 50 km s^{-1}) throughout this period (solid green line in Fig 3iv). v_z (Fig. 3vi), as measured by
293 both C1 and C3 remained low in magnitude ($< 100 \text{ km s}^{-1}$) for the duration of the interval,
294 with a few $v_{\perp z}$ excursions above 100 km s^{-1} observed by C1. The most significant
295 enhancements in $v_{\perp z}$ seen by C1 appeared to occur in conjunction with the rapid current
296 sheet crossings between 00:30:50 and 00:32:00 UT. We discuss the implications of these
297 observations in the context of the upstream IMF conditions and large-scale magnetospheric
298 morphology in section 4.

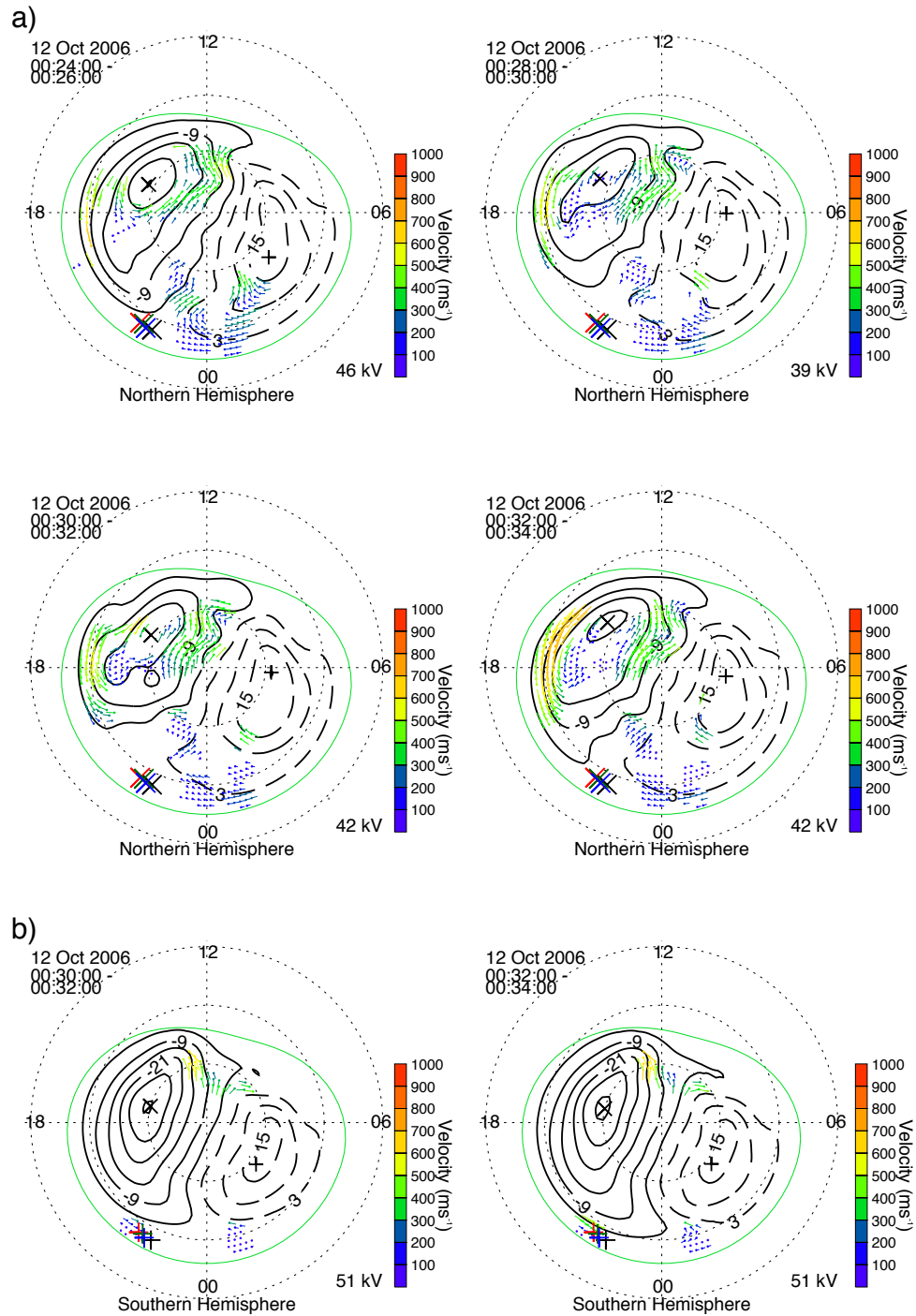
299

300

301 *3.3 Ionospheric Convection Observations*

302

303 To provide the large-scale context in which we can interpret the more localized
304 observations from the Cluster spacecraft we show ionospheric convection observations in
305 Figure 4. In Fig. 4a we present a series of four 2-minute integration SuperDARN maps of the
306 northern hemisphere ionospheric convection pattern, beginning at 00:24 UT, and ending at
307 00:34 UT, which encompasses our specific interval. In all maps, plasma is flowing anti-
308 sunward across the polar cap at high latitudes, also with a strong duskward sense, with the
309 direction of the convection reversing in the pre-midnight sector before returning sunward at
310 lower latitudes.



311

312

313

314

315

316

317

318

Figure 4: Maps of the ionospheric plasma convection derived from SuperDARN observations. Midnight is to the bottom of each map, noon to the top, dusk to the left and dawn to the right. The dashed black circles are spaced every 10° in magnetic latitude. The thicker solid and dashed black lines represent the plasma streamlines and are the contours of the electrostatic potential. Flow vectors are plotted at the locations of radar observations and these are color-coded based on the magnitude of their velocity. a) Four 2-minute northern hemisphere maps from 00:24 – 00:26, 00:28 – 00:30, 00:30 – 00:32 and 00:32 –

319 00:34 UT, respectively. b) Two 2-minute southern hemisphere maps from 00:30 – 00:32 and
320 00:32 – 00:34 UT, respectively. On each northern (southern) hemisphere map, the
321 footpoints of the Cluster spacecraft constellation are shown by the X's (+'s), mapped using
322 the TA15 model.

323

324

325 Owing to the coupled nature of the magnetosphere-ionosphere system, the observed
326 ionospheric convection pattern is indicative of the global-scale magnetospheric convection
327 (Cowley, 1981). In this case, the typical symmetrical twin-cell convection pattern has been
328 rotated clockwise, with the dawn cell extending across into the pre-midnight sector,
329 indicative of convection that has been driven under the influence of a positive IMF B_y
330 component (e.g. Reistad et al., 2016, 2018). On each northern hemisphere map, the
331 footpoints of the Cluster spacecraft constellation are indicated by the crosses (X), mapped
332 using the TA15 model with the same parameterisation described in section 2.

333

334 Fig. 4b shows two 2-minute integration SuperDARN maps of the southern hemisphere
335 ionospheric convection pattern, beginning at 00:30 UT, and ending at 00:34 UT. The
336 associated footpoints of the Cluster spacecraft are indicated by the plus signs (+). Although
337 the coverage of radar data is much less than in the northern hemisphere, there are data in
338 the pre- and post-midnight sectors which appears to be influencing the location of the flow
339 reversal region at the nightside end of the dusk cell. Opposite to the northern hemisphere
340 case, it is the dusk cell in the south which is extending towards, or just beyond, the midnight
341 meridian. This is also consistent with a large-scale positive IMF B_y influence, owing to the
342 expected north-south asymmetry of the influence of IMF B_y in the magnetosphere (e.g.
343 Pettigrew et al., 2010). The significance of these observations is further discussed in section
344 4.1.

345

346 **4. Analysis and Discussion**

347

348 We have presented observations of a dynamic interval of plasma flows and magnetic field in
349 the Earth's magnetotail. In this section we discuss our rationale for interpreting the flows as

350 being inconsistent with large-scale magnetotail untwisting and our interpretation of their
351 relationship to current sheet flapping.

352

353 *4.1 Evidence for an inconsistency with large-scale magnetotail untwisting*

354 During the five-minute interval studied (00:28 – 00:33 UT) C1 measured a continually
355 fluctuating B_x component (Fig. 3i), indicative of multiple crossings of the tail current sheet.
356 C1 was the only spacecraft to measure this signature across the interval (although similar
357 signatures had been observed a few minutes earlier by C2 and C4). C1 also measured a
358 series of earthward convective magnetotail fast flows with varying dusk-dawn components.
359 The data in Fig. 3 i) and Fig. 3 v) illustrate that when B_x was positive (negative), a duskward
360 (dawnward) $v_{\perp y}$ was generally observed. Additionally, the data in Fig. 3 ii) show that C1
361 tended to observe a negative B_y component. According to the magnetotail untwisting
362 hypothesis (e.g. Pitkänen et al., 2015), these flow and magnetic field observations are
363 consistent with a negative IMF B_y penetration. The IMF data presented in Fig. 2a, on the
364 other hand, revealed that IMF B_y was generally positive for several hours prior to the fast
365 flow interval (00:28 – 00:33 UT). Based on the IMF data alone, therefore, one might expect
366 that a positive IMF B_y will have penetrated into the magnetosphere and thus ought to have
367 determined the “expected” dusk-dawn direction of the flow. In that case, the flows
368 observed here would have a dusk-dawn sense that is not explained by current theoretical
369 models of magnetotail untwisting, meaning they are not IMF B_y -controlled (e.g. Grocott et
370 al., 2007). There are a number of possible explanations for this discrepancy and we address
371 each one in turn.

372

373 The first possibility is that our conclusion regarding the expected sense of IMF B_y -control is
374 incorrect. As discussed above, the flows observed by Cluster would be consistent with the
375 magnetotail untwisting hypothesis in the case that we had IMF $B_y < 0$ penetration. We
376 noted in section 3.1 that there were three small negative IMF B_y excursions prior to our
377 Cluster observations interval. Although the propagation of the IMF to the bow shock is
378 accounted for in the OMNI data, there is uncertainty regarding the time it takes for the IMF
379 B_y to ‘propagate’ into the magnetotail. Uncertainties in IMF B_y propagation times (e.g. Case
380 & Wild, 2012) have previously been cited as an explanation for observing an unexpected
381 asymmetry (e.g. Pitkänen et al., 2013). Studies such as Tenfjord et al. (2015, 2017) and Case

382 et al. (2018), for example, have suggested a reconfiguration time (to the prevailing IMF B_y
383 conditions) for nightside closed field lines of around 40 minutes. At \sim 00:28 UT (the
384 beginning of our specific interval of interest), the IMF B_y had been positive for around
385 50 minutes. Based on the Tenfjord timescale, this would thus imply that our interval was
386 wholly IMF $B_y > 0$ driven. Other studies, on the other hand, such as Browett et al. (2017),
387 have shown that longer timescales of a few hours may be important.

388

389 However, for such long timescales to play a role one would expect to have observed a
390 relatively persistent IMF B_y component during that time. The integrated IMF B_y over the
391 hours prior to our interval was certainly convincingly B_y -positive, and it seems highly unlikely
392 that a few minute-long fluctuations into the opposite IMF B_y polarity, 1 or 2 hours prior to
393 the flows we observed, could have a significant influence. We can thus be confident that
394 positive IMF B_y was governing the global magnetospheric dynamics in this case.

395

396 Despite this convincing argument that the IMF data alone imply a positive IMF B_y
397 penetration, we performed an additional analysis to further ensure that these negative
398 excursions did not lead to a change in the global nature of the magnetosphere-ionosphere
399 system. We inspected the concurrent northern hemisphere SuperDARN data (presented in
400 Fig. 4a) to provide evidence of the large-scale convection pattern. If the large-scale flow is
401 consistent with a positive IMF B_y component, then the magnetotail flows that we observed
402 must be deviating from this for some reason and cannot be related to IMF B_y -control. The
403 SuperDARN data indeed confirm that the large-scale morphology of the system was
404 consistent with a positive IMF B_y component (e.g. Lockwood 1993; Grocott et al., 2017;
405 Reistad et al., 2018). This can be inferred from the general shape of the convection pattern,
406 whereby across multiple maps (00:24 – 00:34 UT) the pattern was rotated clockwise, with
407 the dawn cell having extended into the pre-midnight sector. That this is the expected
408 convection pattern for an IMF B_y -driven magnetosphere is also supported by the concurrent
409 low level of geomagnetic activity. The auroral AU and AL indices (not shown) confirm that
410 this interval is geomagnetically quiet (AU and |AL| both less than (or of the order of) 10 nT),
411 such that the nightside ionospheric convection asymmetry should be driven by IMF B_y rather
412 than conductivity-driven features such as the Harang reversal which might otherwise

413 complicate the auroral zone flows (e.g. Grocott et al., 2007; Grocott et al., 2008; Reistad et
414 al., 2018).

415

416 The validity of the convection observations is further supported by the coverage of nightside
417 data which were used to constrain the model convection pattern. The data used to create a
418 SuperDARN convection map are supplemented by data from a statistical model (in this case
419 Ruohoniemi & Greenwald, 1996) which is typically parameterised by the instantaneous IMF
420 conditions. In the case that there is a lack of real data coverage, a created SuperDARN map
421 will be strongly influenced by the model data, as opposed to real data, and thus would
422 reflect a prediction of convection based on the IMF conditions. The maps shown in Fig. 4a
423 illustrate that there were dozens of SuperDARN vectors in the midnight sector which were
424 fitted to create the global convection maps. To confirm that these data were sufficient, and
425 that the observed large-scale convection pattern was not being driven by model data, we
426 parameterised the model in our analysis with IMF $B_y = 0$. Despite this, a clear IMF B_y -
427 asymmetry exists, thus demonstrating that the observed large-scale IMF $B_y > 0$ global
428 convection patterns must be data-driven.

429

430 A second possible explanation for the discrepancy between the dusk-dawn direction of the
431 local and global-scale convection concerns the certainty with which we can determine the
432 location of the spacecraft with respect to the large-scale convection pattern. The untwisting
433 hypothesis, as considered by e.g. Pitkänen et al. (2013, 2017), relies on the assumption that
434 the convection cell to which the spacecraft is connected should be a factor of only
435 hemisphere and the sense of IMF B_y . In other words, as discussed above, for IMF $B_y > 0$, the
436 hypothesis dictates that C1 ought to be located on the dawn cell when above the neutral
437 sheet and the dusk cell when below, at least in the case that the spacecraft is close to
438 midnight (Grocott et al., 2007). This might be true statistically, but does not account for the
439 dusk-dawn location of the spacecraft, which in this case was $6 \lesssim Y \lesssim 7 R_E$. If, as a result, the
440 spacecraft was actually located on the dusk cell when above the neutral sheet, and on the
441 dawn cell when below the neutral sheet, then the sense of the observed plasma sheet flows
442 would actually be consistent with the large-scale convection.

443

444 One way to specify which cell the spacecraft is located within is to map its location into the
445 ionosphere. This has been done using TA15 and is shown by the crosses (X) on the northern
446 hemisphere convection maps and by plus signs (+) on the southern hemisphere convection
447 maps, in Fig. 4a and 4b, respectively. Consider first the northern hemisphere map from
448 00:30 – 00:32 UT in Fig. 4a: the spacecraft appear to map closer to the dawn cell than the
449 dusk cell, such that the predominantly duskward flow that C1 observed in the northern
450 hemisphere plasma sheet would seem to be inconsistent. However, it is worth considering
451 that the pre-midnight location of the spacecraft, the proximity of the mapped footpoints to
452 the dusk cell, and the level of uncertainty generally accepted to be present in field line
453 mapping, may give credence to the possibility that the spacecraft actually mapped to the
454 dusk cell in the northern hemisphere. If this was the case, then the northern hemisphere
455 flows observed by C1 would actually be consistent with the large-scale convection pattern.
456 However, if we consider the southern hemisphere maps in Fig. 4b we can be more certain of
457 which cell the spacecraft map to. Owing to the IMF B_y positive nature of the convection (i.e.
458 the more extended southern hemisphere dusk cell) and the pre-midnight location of the
459 spacecraft, the footpoints are located quite convincingly on the dusk cell. This is despite the
460 dusk-dawn asymmetry being less pronounced than that seen in the northern hemisphere
461 (and the associated poorer coverage of southern hemisphere SuperDARN data). When
462 below the neutral sheet C1 observed downward flows, meaning it would have to have been
463 on the southern hemisphere dawn cell to be consistent with the large-scale convection,
464 which is clearly not the case. Indeed, the observed downward flow in the southern
465 hemisphere at this location could only be interpreted in terms of the untwisting hypothesis
466 for a situation where we had clear IMF $B_y < 0$ penetration (and associated extended dawn
467 cell), which has already been ruled out. C3, meanwhile, continually observed duskward flow,
468 which appears to be consistent with the larger-scale convection. It seems much more likely,
469 therefore, that C1 observed flow that was associated with localized magnetic field dynamics
470 rather than being a signature of the large-scale convection.

471

472

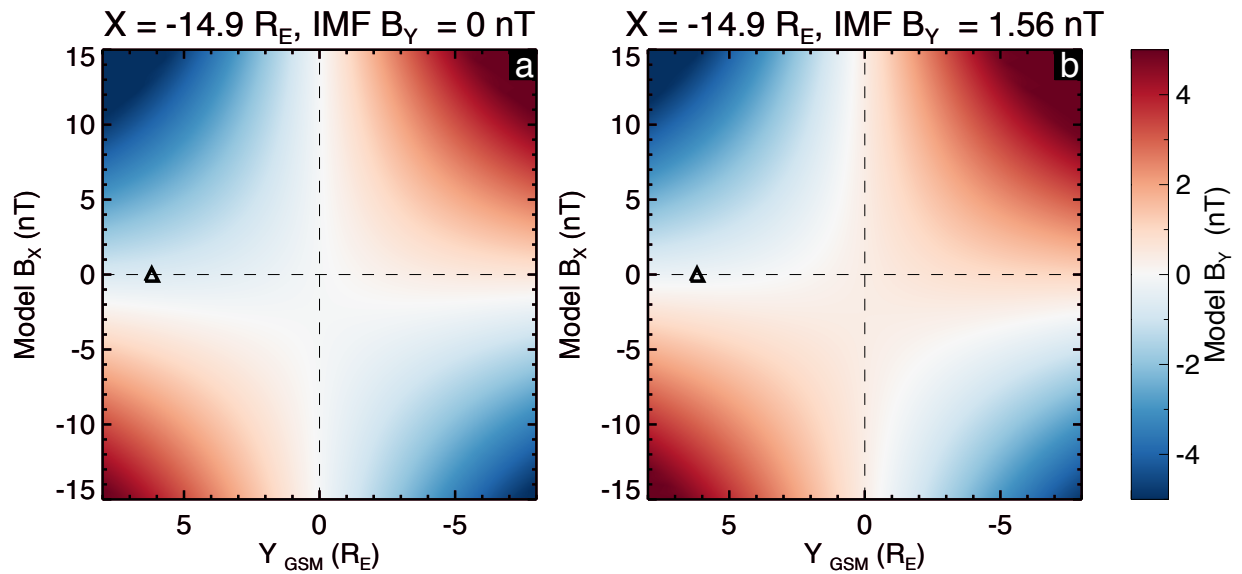
473 *4.2 Evidence for a local perturbation in the magnetotail*

474 The lack of consistency with the large-scale convection leads us to a third explanation for
475 our observations, which is that there is a local perturbation within the tail that is

476 independent of any large-scale, IMF B_y -controlled asymmetry associated with magnetotail
477 untwisting. This is supported by the observations from the other Cluster spacecraft. The
478 low-level of flow seen by C3 is mostly duskward (Fig. 3v) and therefore consistent with the
479 idea of untwisting under IMF $B_y > 0$, given its southern hemisphere location; although, it
480 should be noted that this observation would also be consistent with the expected duskward
481 flow in a pre-midnight location even in the absence of a large-scale asymmetry (e.g.
482 Kissinger et al., 2012). Further, in Fig. 2b v), up until the rapid B_x variations began at $\sim 00:24$
483 UT, fast duskward flow in the southern hemisphere was also seen by C1. The fact that C3
484 continued to then observe steady duskward flow, and no significant B_x change, suggests
485 that the change in the nature of the C1 observations after 00:24 UT must in-fact be due to
486 some localized process that was responsible for driving the dawnward component of the
487 flows which was only observed by C1.

488

489 This idea of a local perturbation is also supported by the variations in the local B_y
490 component. Fig. 3 ii) illustrates the in-situ variations in B_y with time across the interval.
491 Despite there clearly being positive IMF B_y penetration globally (as confirmed by inspection
492 of the OMNI and SuperDARN data), C1, C2 and C4 all recorded mostly negative local B_y
493 values. In the studies of, e.g., Pitkänen et al. (2013, 2017) this observation would have been
494 offered as evidence of a negative of IMF B_y penetration, thus supporting the untwisting
495 hypothesis. However, it is important to note that a negative local B_y component may be
496 wholly consistent with positive IMF B_y . There are, in fact, multiple sources of B_y in the tail,
497 such as magnetotail flaring (Fairfield, 1979), as well as tilt effects and current sheet warping
498 (see e.g. Petrukovich et al., 2005), in addition to a penetration of the IMF B_y . To fully
499 interpret the magnetic field observations, we must therefore consider the possible effects
500 of these phenomena on the presence of B_y in the tail at the specific location of each
501 spacecraft.



502
503

504 **Figure 5:** TA15 model magnetic field data. In each case, plotted is Y vs B_x [GSM], (at
505 $X = -14.9 R_E$, i.e. the X position of C1 at $\sim 00:28$ UT on 12 Oct 2006), with the TA15 modelled
506 B_y value shown by the color bar on the right. The black triangle shows the Y -location of C1,
507 at $B_x = 0$. In panel (a) we have imposed IMF $B_y = 0$, and for panel (b) we have used the 1-
508 hour mean-averaged IMF B_y (+1.56 nT) in the hour prior to 00:28 UT.

509

510 To aid in this interpretation, we present TA15 model magnetic field data in Figure 5, to
511 provide an indication of the expected background B_y -component at the time of our interval.
512 These data, from $X = -14.9 R_E$, are plotted against Y [GSM]-position on the horizontal axis,
513 and against the B_x -component on the vertical axis. We have reversed the conventional
514 direction of the horizontal axis (negative to positive from left to right) to be consistent with
515 a view looking earthward from downtail. In panel (a) we show the field for the case that IMF
516 $B_y = 0$ and in panel (b) the case that IMF $B_y = +1.56$ nT (the 1-hour mean-averaged IMF B_y in
517 the hour prior to 00:28 UT). The first conclusion we can make from consideration of the B_y
518 component in Fig. 5a is how, even under no IMF B_y penetration, a ‘background’ B_y value will
519 exist in the tail purely dependent on location. In such a ‘symmetric’ tail, one would expect
520 the background B_y value to appear as one moves away from midnight toward the dusk-
521 dawn flanks, as well as further above and below the neutral sheet. Pre-midnight, we would
522 expect to observe negative B_y above the neutral sheet ($B_x > 0$), and positive B_y below the

523 neutral sheet ($B_x < 0$), with the opposite effect post-midnight. This is the well known
524 magnetotail flaring effect (Fairfield, 1979).

525

526 The data in Fig. 5a also show the effect of the negative (tailward) dipole tilt (as appropriate
527 to our study interval) and current sheet warping on the local B_y component. According to
528 Petrukovich (2011), the current sheet warping (controlled by the dipole tilt) is expected to
529 add a negative B_y component pre-midnight and a positive B_y component post-midnight.

530 Furthermore, the ‘even tilt’ effect is expected to add a negative B_y component to both the
531 pre and post-midnight sectors for a negative tilt. This leads to the effect seen in Fig. 5a
532 where in the pre-midnight sector, the location of the B_y polarity change occurs in the
533 southern hemisphere (at $B_x \approx -3$ nT).

534

535 Fig. 5b illustrates the scenario relevant to our case study, where we have additionally a
536 global positive IMF B_y penetration. This additional positive B_y has the effect of moving the
537 location of the pre-midnight B_y polarity change back up towards the neutral sheet. This
538 explains why the Cluster spacecraft observed $B_y \approx 0$ at times of $B_x \approx 0$ during the few tens of
539 minutes prior to our interval, as noted in section 3.2. This also explains why C2-3 and C4
540 observed the polarity of B_y that they did throughout the interval. It is thus clear that positive
541 IMF B_y penetration does not mean we should expect to observe positive B_y everywhere in
542 the tail, rather, it simply means that there is expected to be some positive B_y perturbation
543 to the already present ‘background’ B_y at a particular location. As Fig. 5b demonstrates, C2
544 and C4 (located above the neutral sheet) are expected to have observed negative B_y even
545 though positive IMF B_y has penetrated into the magnetotail, illustrating that the flaring
546 effect is generally dominant at the spacecraft location. The background B_y expected at their
547 location (pre-midnight, $B_x > 0$), is negative and the IMF B_y -associated perturbation was not
548 large enough to enforce a sign change in B_y .

549

550 The Cluster spacecraft in our study were all located pre-midnight (+Y GSM). From Figure 3,
551 C2 and C4 observed positive B_x , and negative B_y , and at ~00:28 UT were located at around
552 $Z = -1 R_E$ (Figure 1). C3, however, observed negative B_x and positive B_y , and was located at
553 around $Z = -2.5 R_E$. The location of the neutral sheet at ~00:28 UT can therefore be said
554 (locally) to have been somewhere between -1 and $-2.5 R_E$ in Z . C1 was located at around $Z =$

555 $-1.5 R_E$ and, throughout the five-minute interval, observed a B_x which continually fluctuated
556 from positive to negative, yet observed mostly weakly negative B_y . For B_y to have remained
557 negative, despite C1 moving above and below the neutral sheet, suggests that there was a
558 B_y negative ‘kink’ in the magnetotail that was localized to the vicinity of C1. This is further
559 supported by the fact that numerous (albeit brief) positive B_y excursions occurred when C1
560 was above the neutral sheet (as noted in section 3.2). We use the term ‘kink’ to highlight a
561 deformation in the nearby field lines which results in the observed perturbations to the local
562 B_y component. We suggest that this deformation could be relatively small in terms of field
563 line length, much like a kink in a cable or wire. In the following section, we investigate this
564 kink in relation to the observed current sheet flapping.

565

566

567 *4.3 Evidence for current sheet flapping as a source of the asymmetric flows*

568 If a localized magnetic field perturbation was associated with the lack of observation of the
569 expected dusk-dawn flow for magnetotail untwisting, investigating its cause seems a
570 worthwhile endeavour. The clear sinusoidal-like variation in B_x observed by C1, which is
571 evidence of current sheet flapping (e.g. Runov et al., 2009), provides us with a starting point
572 for this investigation. This flapping must be highly localized as at the time of our five-minute
573 flow interval (00:28 -00:33 UT), only C1 observed the flapping. MVA analysis (Sonnerup &
574 Cahill, 1967) suggests that the flapping was a kink-like wave which was propagating
575 dawnward (Rong et al., 2015; Wu et al., 2016), and therefore may have been a source of the
576 observed dusk-dawn flow.

577

578 The causes of current sheet flapping have been discussed previously (Runov et al., 2009;
579 Wei et al., 2019). One such cause has been attributed to localized, periodical reconnection –
580 a process known to drive Bursty Bulk Flows (BBFs) in the magnetotail (Angelopoulos et al.,
581 1994; Zhang et al., 2016). In fact, BBFs excited directly as a result of reconnection in the tail
582 have been previously linked to magnetic fluctuations in the current sheet (Nakamura et al.,
583 2009; Wu et al., 2016). Examining the data presented in Fig. 3 iii) and Fig. 3 iv), we note that
584 C1 measured a generally positive B_z , with a few negative blips, as well as continually fast (v_x
585 $> 200 \text{ km s}^{-1}$) earthward flow, peaking at over 370 km s^{-1} with bursts of enhanced
586 convective flow ($v_{\perp x} > 200 \text{ km s}^{-1}$) also apparent. These observations are fairly consistent

587 with (if slightly slower than) the original definition of a BBF (Angelopoulos et al., 1994). This,
588 along with the absence of similar flow observations in the C3 data, suggests that C1 may
589 have been located earthward of a localized reconnection site (owing to $B_z > 0$), where
590 persistent, localized reconnection was exciting fast earthward flow. The reconnection
591 process may then have been driving the current sheet flapping, inducing the localized kink in
592 the field, and ultimately controlling the dusk-dawn direction of the convective flow.

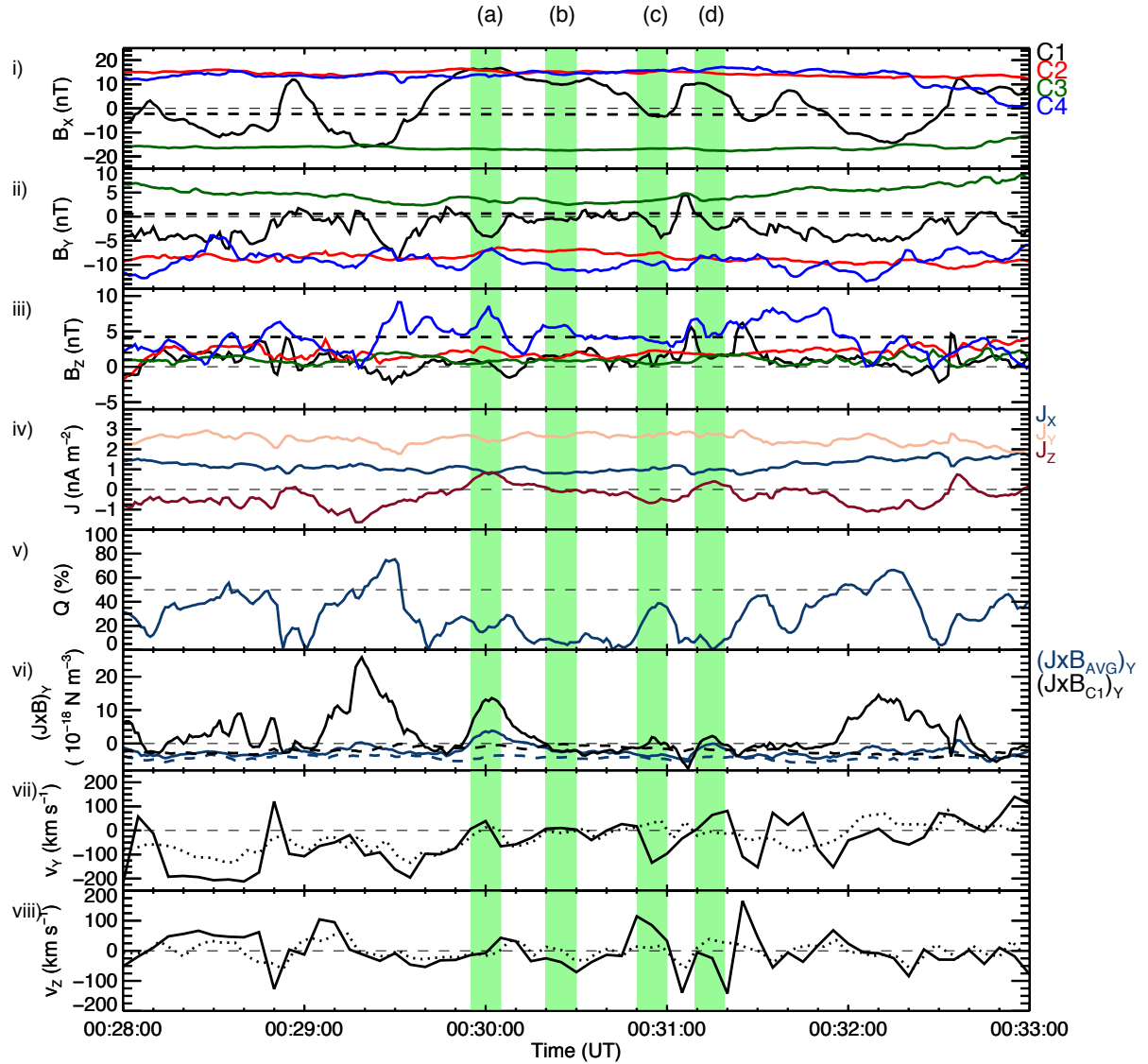
593

594

595 It is well known that the magnetic tension force is responsible for the acceleration of plasma
596 following reconnection (Karlsson et al., 2015). Our observations of a dusk-dawn flow
597 component may be related to the localized magnetic tension forces driving and directing
598 plasma flows in association with the flapping. In order to provide some scope to this
599 suggestion, we attempted to find the direction of the $\mathbf{J} \times \mathbf{B}$ forces acting on the plasma. We
600 used the curlometer technique (Dunlop et al., 1988, 2002), to estimate the average current
601 density, \mathbf{J} , flowing through the volume bound by the spacecraft tetrahedron. The $\mathbf{J} \times \mathbf{B}$
602 force density [N m^{-3}] is then calculated, firstly, by taking the cross product of \mathbf{J} with the
603 average magnetic field vector \mathbf{B} from the four-spacecraft (\mathbf{B}_{AVG}). We also calculate $\mathbf{J} \times \mathbf{B}$
604 using solely \mathbf{B} from C1 (\mathbf{B}_{C1}), in order to provide a more local estimate for $\mathbf{J} \times \mathbf{B}$ at the
605 location of C1.

606

607 In order to check the validity of using the curlometer approach, we calculated the quality
608 parameter, Q , defined as $|\nabla \cdot \mathbf{B}|/|\nabla \times \mathbf{B}|$. It is generally accepted that a value of $Q < 0.5$ is
609 required for a current estimate to be valid. Hence, the value of Q , along with due
610 consideration of the spacecraft configuration and its orientation relative to the magnetic
611 field structure, may be used as a monitor of how reliable the curlometer approach is
612 (Dunlop et al., 2002). This is discussed further below, in reference to the analysis shown in
613 Figure 6.



614

615 **Figure 6:** i-iii) The local magnetic field vector \mathbf{B} (B_x , B_y , B_z) observed by C1-4, as shown
 616 previously (solid lines) and the TA15 modelled \mathbf{B} vector for C1 (dashed black lines). iv) The
 617 components of the current density vector \mathbf{J} (J_x , J_y , J_z), v) Q , vi) $(\mathbf{J} \times \mathbf{B}_{AVG})_y$ (solid blue line)
 618 and $(\mathbf{J} \times \mathbf{B}_{C1})_y$ (solid black line). The dashed blue and black lines indicate the equivalent
 619 calculation where the TA15 model \mathbf{B} field of C1 has been used (see text). vii) v_y ($v_{\perp y}$ in solid
 620 lines), observed by C1 and viii) v_z ($v_{\perp z}$ in solid lines), also observed by C1. The green
 621 highlighted regions labelled (a), (b), (c) and (d) correspond to four specific time-windows of
 622 interest (discussed in-text).

623

624 Shown in Fig. 6 i-iii) are the local magnetic field B_x , B_y and B_z components, as presented
 625 previously. In Fig. 6 iv) are the current density J_x , J_y and J_z components determined from the

626 curlometer analysis. In Fig. 6 vi) is the dusk-dawn component of $\mathbf{J} \times \mathbf{B}_{AVG}$ and $\mathbf{J} \times \mathbf{B}_{C1}$.
 627 Finally, in Fig. 6 vii) and viii) are the dusk-dawn and north-south components of the flow
 628 (and field-perpendicular flow) observed by C1, as shown previously. In panels (i-iii), the
 629 dashed black line represents the TA15 modelled magnetic field (see section 4.2) at the
 630 location of C1. In panel (vi) the dashed blue and black lines represent the $(\mathbf{J} \times \mathbf{B}_{AVG})_y$ and $(\mathbf{J}$
 631 $\times \mathbf{B}_{C1})_y$ forces, respectively, where \mathbf{J} and $\mathbf{J} \times \mathbf{B}$ have been computed using the model field
 632 at the location of C1 and the true magnetic fields measured by C2-C4. These ‘model $(\mathbf{J} \times \mathbf{B})_y$
 633 forces’ have been computed to provide an illustration of what one would expect the
 634 ‘unperturbed’ magnetic field of C1 and the associated $(\mathbf{J} \times \mathbf{B})_y$ force to look like, in the
 635 absence of any dynamical effects such as current sheet flapping or field line ‘kinking’. In
 636 both cases, the model $(\mathbf{J} \times \mathbf{B})_y$ forces are weakly downward, consistent with the
 637 ‘background curvature’ of the magnetic field at this pre-midnight location (see Fig. 7). Fig. 6
 638 v) suggests that our curlometer approach is generally appropriate, as Q mostly remains
 639 below 50% (horizontal dashed line) for the five-minute interval. We note that, unlike in
 640 previous studies which have used the curlometer technique at inter-spacecraft separation
 641 distances of $\ll 1 R_E$ (e.g. Dunlop et al., 2002; Runov et al., 2003), in our case the Cluster
 642 spacecraft separation is large ($\gtrsim 1 R_E$). Therefore, the curlometer is likely to be an
 643 underestimate of the true current at these scale sizes. Critically, however, the spacecraft
 644 configuration is such that the estimate of the direction of the currents should be stable.
 645 Thus, although the volume enclosed by the spacecraft is greater than the scale sizes of the
 646 current sheet flapping and kink, a reliable estimate of the direction of the net $\mathbf{J} \times \mathbf{B}$ force
 647 within the enclosed volume may still be obtained.

648
 649 Two key features of Figure 6 are apparent. Firstly, it appears as though the perturbations to
 650 $(\mathbf{J} \times \mathbf{B})_y$ are mostly associated with the magnetic field perturbations generally only observed
 651 by C1. This is made apparent by comparing $(\mathbf{J} \times \mathbf{B}_{C1})_y$ with $(\mathbf{J} \times \mathbf{B}_{AVG})_y$, where the
 652 perturbations are much larger in magnitude for $(\mathbf{J} \times \mathbf{B}_{C1})_y$. We also note that both
 653 $(\mathbf{J} \times \mathbf{B}_{AVG})_y$ and $(\mathbf{J} \times \mathbf{B}_{C1})_y$ are effectively always positive with respect to their model
 654 equivalents. However, $(\mathbf{J} \times \mathbf{B}_{AVG})_y$ is still mostly net negative whereas $(\mathbf{J} \times \mathbf{B}_{C1})_y$ is net
 655 positive. This suggests that using \mathbf{B}_{C1} , rather than \mathbf{B}_{AVG} in calculating $(\mathbf{J} \times \mathbf{B})_y$ has overall

656 reduced the effects of the larger-scale background field curvature (incorporated by
 657 including the other spacecraft). Second, the magnetic field and flow dynamics evident in Fig.
 658 6 appear to almost always be associated with positive (duskward) enhancements in $(\mathbf{J} \times \mathbf{B})_y$,
 659 in contrast to the model dawnward sense of $(\mathbf{J} \times \mathbf{B})_y$. This is particularly evident in the case
 660 of $(\mathbf{J} \times \mathbf{B}_{C1})_y$, but also generally true in the case of $(\mathbf{J} \times \mathbf{B}_{AVG})_y$. We therefore suggest that
 661 the dynamic behaviour of $(\mathbf{J} \times \mathbf{B})_y$ is simply consistent with the localised kinks and flapping
 662 in the magnetic field that are associated with the transient perturbations to the dusk-dawn
 663 flow observed by C1.

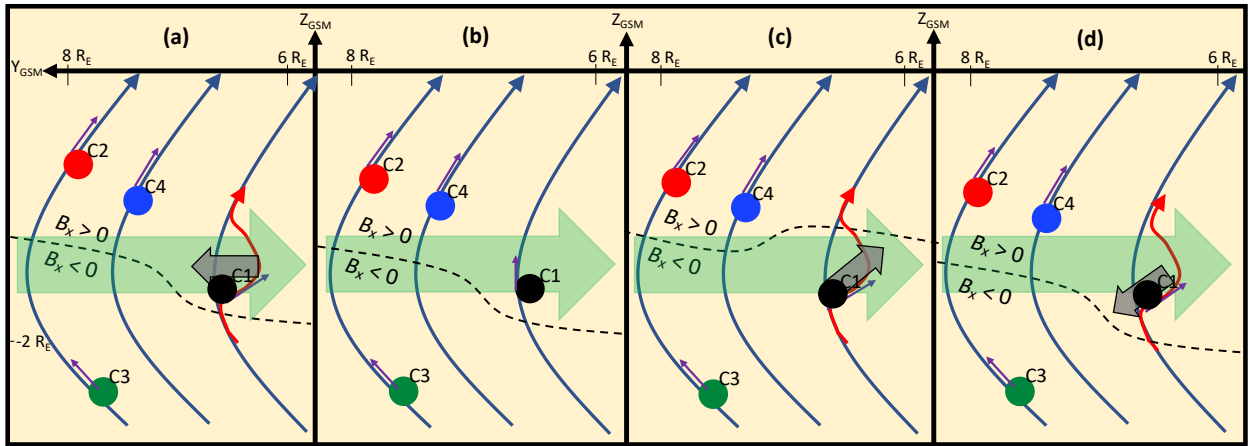
664

665

666 *4.4 Visualization of the observed dynamics*

667 In an effort to visualize these plasma sheet dynamics, we show in Figure 7 a series of
 668 sketches that attempt to associate the observed magnetic field perturbations with the
 669 observed dusk-dawn convective flows. The panels correspond to the four time-windows
 670 indicated on Figure 6 by the highlighted regions labelled a-d. In each panel, we indicate the
 671 approximate relative position of the 4 Cluster spacecraft in GSM coordinates, and the
 672 appropriate sense of B_y measured by each spacecraft is shown by the purple arrows at each
 673 spacecraft location (the Z-component of the field was in fact generally small, and has been
 674 exaggerated here for illustrative purposes). We also superimpose nominal plasma sheet
 675 field lines (again with an exaggerated extent in Z) that display the sense of B_y implied by the
 676 TA15 data presented in Figure 5 (long blue curved arrows). The dashed lines represent the
 677 location of the neutral sheet at the end of each time window. This is tilted slightly, as
 678 appropriate for IMF $B_y > 0$, but with the end-state of the “flap” of the current sheet implied
 679 by the sign of B_x observed by C1. In red is the perturbation to the field implied by the sign of
 680 B_y observed by C1.

681



682

683

684 **Figure 7:** Schematic diagrams of the observed magnetic field perturbations and dusk-dawn

685 convective flows during the time-windows indicated in Fig. 6 by the highlighted regions. The

686 approximate locations of the four Cluster spacecraft relative to one-another in the Y-Z GSM

687 plane are indicated (not to scale) by the colored circles. The curved blue arrows represent

688 magnetic field lines, and the short purple arrow indicates the local sense of B_y at the

689 location of each spacecraft. The dashed black line indicates the current sheet. In panels (a),

690 (b) and (d), the curved red arrow shows the 'kinked' magnetic field line. The long thick green

691 arrow shows the direction of the model $(\mathbf{J} \times \mathbf{B})_y$ force associated with the background

692 curvature of the magnetic field, and the small thick gray arrow shows the direction of the

693 dusk-dawn convective flow observed by C1.

694

695

696 In Fig. 7a C1 is located above the current sheet and measured negative B_y . A weakly

697 duskward convective flow was observed at this time (as indicated by the thick gray arrow),

698 consistent with the duskward sense of the $(\mathbf{J} \times \mathbf{B})_y$ force, and opposite to the sense of the

699 model $(\mathbf{J} \times \mathbf{B})_y$ force associated with the background curvature of the magnetic field. In Fig.

700 7b, C1 is still above the current sheet but measured $B_y \approx 0$ and no dusk-dawn convective

701 flow. In Fig. 7c C1 is shown below the current sheet, where the background B_y would be

702 positive (see Fig. 5b). C1 instead observed an increasingly negative B_y , which we suggest is

703 associated with the presence of the kink in the field. At the same time, C1 also observed a

704 convective plasma flow with downward and slightly upward (+Z) component (thick gray

705 arrow). We therefore suggest that the flow was associated with the upward/dawnward flap
 706 of the current sheet, and that the dawnward sense of the flow likely also resulted in the
 707 increase in negative B_y seen during the time-window shown in Fig. 6c. The positive
 708 $(\mathbf{J} \times \mathbf{B}_{C1})_y$ at this time, whilst inconsistent with the dawnward sense of the flow, is therefore
 709 consistent with the curvature of the magnetic field associated with the kink. $(\mathbf{J} \times \mathbf{B}_{AVG})_y$,
 710 meanwhile, was negative, likely due to incorporating the larger-scale background curvature
 711 of the magnetic field observed by the other spacecraft. In Fig. 7d C1 is shown above the
 712 current sheet, where it observed a weakly negative B_y . In this case, C1 observed a
 713 convective plasma flow with duskward and slightly downward ($-Z$) component. Similarly to
 714 in Fig. 7a, this flow occurred in concert with a positive enhancement in $(\mathbf{J} \times \mathbf{B})_y$ relative to
 715 the model $(\mathbf{J} \times \mathbf{B})_y$. This flow would therefore seem to be associated with the downward
 716 flap of the current sheet, and its duskward sense could indicate that it is acting to reduce
 717 the negative kink in B_y that is apparent over the time-window shown in Fig. 6d.

718

719 Whilst we acknowledge a degree of uncertainty in the details of the interpretation
 720 presented above of the specific relationship between the flows and the field, it serves to
 721 illustrate three observations about this interval of which we can be very certain: 1) The IMF,
 722 ionospheric convection, and comparison of the plasma sheet magnetic field observations to
 723 the TA15 model field, all lead to the expectation of an IMF $B_y > 0$ large-scale asymmetry in
 724 the magnetosphere. 2) The Cluster 1 spacecraft observed convective flow with a dusk-dawn
 725 component that was inconsistent with current theories of IMF B_y -induced dusk-dawn flows
 726 associated with magnetotail untwisting. We therefore note that the observations presented
 727 here cannot be attributed to the current model of large-scale magnetotail untwisting. 3)
 728 Magnetic field perturbations that were indicative of a localized current sheet flapping and
 729 dusk-dawn kink in the field occurred coincident with the flows. It therefore seems likely that
 730 in this case the IMF B_y -driven asymmetry was insufficient to override the localised dynamics
 731 in governing the dusk-dawn component of the flow.

732

733

734

735

736 **5. Summary**

737

738 We have presented a case study from 12 October 2006 revealing a dynamic interval of
739 plasma flows and current sheet flapping, observed by the Cluster 1 spacecraft. The key
740 observations presented in this study may be summarised as follows:

741

- 742 • The OMNI data revealed that the IMF B_y had been positive for several hours prior to
743 our interval of Cluster data, with the exception of three short-lived negative
744 excursions.
- 745 • The SuperDARN ionospheric convection observations revealed a large-scale
746 asymmetry consistent with IMF $B_y > 0$.
- 747 • C1 observed a changing B_x magnetic field component and associated duskward ($v_{\perp y}$
748 > 0) flow when in the northern magnetic hemisphere, and dawnward ($v_{\perp y} < 0$) flow
749 in the southern magnetic hemisphere.

750

751 Contrary to the results of a number of previous studies in the literature, during this
752 particular interval, the dusk-dawn sense of the convective magnetotail flows ($v_{\perp y}$); and in
753 particular, the dawnward flow observed in the southern hemisphere, does not agree with
754 expectations based on the theoretical understanding of global magnetotail untwisting and
755 the prevailing positive IMF B_y conditions, nor to expectations based on the location of the
756 spacecraft and associated magnetotail flaring. We instead attribute the flows to a localized
757 magnetic field perturbation, or 'kink' in the magnetotail, which appears to have been
758 independent of any large-scale dynamics and may have instead been related to the
759 observed current sheet flapping. We attributed the current sheet flapping to being driven
760 by localized reconnection, itself inferred from the presence of the observed bursty fast
761 earthward flow ($v_{\perp x} \approx 200 \text{ km s}^{-1}$). Analysis using the curlometer technique suggests that
762 the $(\mathbf{J} \times \mathbf{B})_y$ force is consistent with the localised kinks and flapping in the magnetic field
763 that are associated with the transient perturbations to the dusk-dawn flow observed by C1.

764

765

766 Although evidence for the large-scale penetration of IMF $B_y > 0$ is apparent, the IMF $B_y > 0$
 767 penetration at the location of C1 appears to have been unable to override the variable dusk-
 768 dawn flow associated with the current sheet flapping. Further studies by the authors are
 769 currently underway to determine if such flows are a frequent occurrence, and to consider,
 770 and account for, localized tail dynamics more fully in a statistical analysis of the magnetotail
 771 flows.

772

773 **Acknowledgements**

774

775 The authors would like to thank the FGM and CIS teams as part of the Cluster mission and
 776 acknowledge the Cluster Science Archive (Laakso et al., 2010) as the source of the Cluster
 777 data. We also wish to thank the OMNIWeb as the source of the solar wind and IMF data.
 778 The authors acknowledge the use of SuperDARN data. SuperDARN is a collection of radars
 779 funded by national scientific funding agencies of Australia, Canada, China, France, Italy,
 780 Japan, Norway, South Africa, United Kingdom, and United States of America, and we thank
 781 the international PI team for providing the data. The authors acknowledge access to the
 782 SuperDARN database via BAS data mirror (<http://bslsuperdarn.nc.nerc-bas.ac.uk:8093/docs/>)
 783 and are grateful for use of the Radar Software Toolkit (RST v4.2
 784 <https://zenodo.org/record/1403226#.Xy0u7y3MxTY>) with which the raw radar data were
 785 processed. We acknowledge the WDC for Geomagnetism, Kyoto, for use of the auroral
 786 electrojet indices, which may be obtained from <http://wdc.kugi.kyoto-u.ac.jp/aedir/>. We are
 787 also grateful to Haje Korth for providing the IDL Geopack DLM containing the Tsyganenko
 788 magnetic field model routines and coordinate system conversions and wish to thank Nikolai
 789 Tsyganenko for useful discussion of his magnetic field models. Finally, we are thankful for
 790 the advice of Malcolm Dunlop regarding the applicability of the curlometer technique at
 791 large spacecraft separations. This research was undertaken with the support of funding
 792 from the following sources: Lancaster University Faculty of Science and Technology
 793 studentship (JHL), STFC Consolidated grant no. ST/R000816/1 (NAC, AG), NERC standard
 794 grant nos. NE/P001556/1 and NE/T000937/1 (MTW, AG).

795

796 **References**

797

798 Angelopoulos, V., Baumjohann, W., Kennel, C. F., Coroniti, F. V., Kivelson, M. G., Pellat, R.,
 799 Walker, R. J., Lühr, H. and Paschmann, G. (1992). Bursty bulk flows in the inner central
 800 plasma sheet. *J. Geophys. Res.*, *97 (A4)*, 4027-4039. doi:10.1029/91JA02701

801

802 Angelopoulos, V., Kennel, C. F., Coroniti, F. V., Pellat, R., Kivelson, M. G., Walker, R. J.,
 803 Russell, C. T., Baumjohann, W., Feldman W. C. and Gosling, J. T. (1994). Statistical
 804 characteristics of bursty bulk flow events. *J. Geophys. Res.*, *99 (A11)*, 21,257-21,280.
 805 doi:10.1029/94JA01263

806

807 Balogh, A., Carr, C. M., Acuña, M. H., Dunlop, M. W., Beek, T. J., Brown, P., Fornacon, K. -H.,
 808 Georgescu, E., Glassmeier, K. -H., Harris, J., Musmann, G., Oddy, T. and Scwingenschuh, K.

- 809 (2001). The Cluster magnetic field investigation: Overview of in-flight performance and
810 initial results. *Ann. Geophys.*, *19*, 1207-1217. doi: 10.5194/angeo-19-1207-2001
811
- 812 Baumjohann, W., Paschmann, G. and Cattell, C. A. (1989). Average Properties in the Central
813 Plasma Sheet. *Journal of Geophysical Research*, *94 (A6)*, 6597-6606. doi:
814 10.1029/JA094iA06p06597
815
- 816 Browett, S. D., Fear, R. C., Grocott, A., and Milan, S. E. (2017). Timescales for the penetration
817 of IMF B_y into the Earth's magnetotail. *J. Geophys. Res.: Space Physics*, *122 (1)*, 579-593.
818 doi:10.1002/2016JA023198
819
- 820 Cao, J. B., Ma, Y. D., Parks, G., Rème, H., Dandouras, I., Nakamura, R., Zhang, T. L., Zong, Q.,
821 Lucek, E., Carr, C. M., Liu, Z. X. and Zhou, G. C. (2006). Joint observations by Cluster satellites
822 of bursty bulk flows in the magnetotail. *J. Geophys. Res.*, *111 (A4)*, A04206.
823 doi:10.1029/2005JA011322
824
- 825 Case, N. A., Grocott, A., Haaland, S., Martin, C. J., and Nagai, T. (2018). Response of the
826 Earth's Neutral Sheet to Reversals in the IMF B_y component. *J. Geophys. Res.*, *123 (10)*,
827 8206-8218. doi:10.1029/2018JA025712
828
- 829 Case, N. A. and Wild, J. (2012). A statistical comparison of solar wind propagation delays
830 derived from multispacecraft techniques. *J. Geophys Res.*, *117 (A2)*, A02101,
831 doi:10.1029/2011JA016946.
832
- 833 Chisham G., Lester, M., Milan, S. E., Freeman, M. P., Bristow, W. A., Grocott A., McWilliams,
834 K. A., Ruohoniemi, J. M., Yeoman, T. K., Dyson, P. L., Greenwald, R. A., Kikuchi, T., Pinnock,
835 M., Rash, J. P. S., Sato, N., Sofko, G. J., Villain, J. -P. and Walker, A. D. M. et al. (2007). A
836 decade of the Super Dual Auroral Radar Network (SuperDARN): scientific achievements,
837 new techniques and future directions. *Surveys in Geophysics* *28*, 33-109.
838 doi:10.1007/s10712-007-9017-8
839
- 840 Cowley, S. W. H. (1981). Magnetospheric asymmetries associated with the y -component of
841 the IMF. *Planet Space Sci*, *29 (1)*, 79-96. doi:10.1016/0032-0633(81)90141-0
842
- 843 Dungey, J. W. (1961). Interplanetary magnetic field and the auroral zones. *Phys. Rev. Lett.*, *6*,
844 47-48. doi:10.1103/PhysRevLett.6.47
845
- 846 Dunlop, M. W., Southwood, D. J., Glassmeier, K. -H., and Neubauer, F. M. (1988). Analysis of
847 multipoint magnetometer data. *Advances in Space Research*, *8 (9-10)*, 273-277.
848 doi:10.1016/0273-1177(88)90141-X
849
- 850 Dunlop, M. W., Balogh, A., Glassmeier, K. -H. and Robert, P. (2002). Four-point Cluster
851 application of magnetic field analysis tools: The Curlometer. *J. Geophys. Res.*, *107 (A11)*.
852 doi:10.1029/2001JA005088
853
- 854 Escoubet, C. P., Fehringer, M. and Goldstein, M. (2001). The Cluster Mission. *Ann. Geophys.*,
855 *19*, 1197 – 1200. doi:10.5194/angeo-19-1197-2001

856

857 Fairfield, D. H. (1979). On the Average Configuration Of The Geomagnetic Tail. *J. Geophys.*
858 *Res.*, 84 (A5), 1950-1958. doi:10.1029/JA084iA05p01950

859

860 Frühauff, D. and Glassmeier, K.-H. (2016). Statistical analysis of magnetotail fast flows and
861 related magnetic disturbances. *Ann. Geophys.*, 34, 399-409. doi:10.5194/angeo-34-399-
862 2016

863

864 Grocott, A. (2017). Time Dependence of Dawn-Dusk Asymmetries in the Terrestrial
865 Ionospheric Convection Pattern. In: Haaland, S. et al. (2017), *Dawn-Dusk Asymmetries in*
866 *Planetary Plasma Environments*, John Wiley and Sons, Inc., 107-123

867

868 Grocott, A., Yeoman, T. K., Nakamura, R., Cowley, S. W. H, Frey, H. U., Rème, H. and Klecker,
869 B. J. (2004a). Multi-instrument observations of the ionospheric counterpart of a bursty bulk
870 flow in the near-Earth plasma sheet. *Ann. Geophys.*, 22, 1061-1075, 1432-0576/ag/2004-22-
871 1061.

872

873 Grocott, A., Yeoman, T. K., Cowley, S. W. H, and Rème, H. (2004b). Multi-instrument
874 observations of bursty bulk flows and their ionospheric counterparts. *Proc. Seventh Internat.*
875 *Conf. on Substorms*, UDK-52-854, FMI, Helsinki, Finland, 107-110.

876

877 Grocott, A., Badman, S. V., Cowley, S. W. H, and Cripps (2004c). The influence of the IMF B_y
878 on the nature of the nightside high-latitude ionospheric flow during intervals of positive IMF
879 B_z . *Ann. Geophys.*, 22, 1755-1764, doi:10.5194/angeo-22-1755-2004.

880

881 Grocott, A., Yeoman, T. K., Milan, S. E. and Cowley, S. W. H. (2005), Interhemispheric
882 observations of the ionospheric signature of tail reconnection during IMF-northward non-
883 substorm intervals, *Ann. Geophys.*, 23, 1763–1770. doi:10.5194/angeo-23-1763-2005.

884

885 Grocott, A., Yeoman, T. K., Milan, S. E., Amm, O., Frey, H. U., Juusola, L., Nakamura, R.,
886 Owen, C. J., Rème, H. and Takada, T. (2007). Multi-scale observations of magnetotail flux
887 transport during IMF-northward non-substorm intervals. *Ann. Geophys.*, 25, 1709-1720.
888 doi:10.5194/angeo-25-1709-2007

889

890 Grocott, A., Milan, S. E. and Yeoman, T. K. (2008). Interplanetary magnetic field control of
891 fast azimuthal flows in the nightside high-latitude ionosphere, *Geophys. Res. Lett.*, 35,
892 L08102, doi:10.1029/2008GL033545.

893

894 Haaland, S., Runov, A. and Forsyth, C. (2017). Dawn-Dusk Asymmetries in Planetary Plasma
895 Environments, *Geophysical Monograph 230, First Edition. American Geophysical Union.*
896 Published 2017 by John Wiley & Sons, Inc.

897

898 Karlsson, T., Hamrin, M., Nilsson, H., Kullen, A., and Pitkänen, T. (2015). Magnetic forces
899 associated with bursty bulk flows in the Earth's magnetotail. *Geophys. Res. Lett.*, 42 (9),
900 3122-3128. doi:10.1002/2015GL063999

901

- 902 Kiehas, S. A., Runov, A., Angelopoulos, V., Hietala, H. and Korovinskiy, D. (2018). Magnetotail
903 Fast Flow Occurrence Rate and Dawn-Dusk Asymmetry at $X_{GSM} \sim -60 R_E$. *J. Geophys. Res.:*
904 *Space Physics*, *123* (3), 1767 – 1778. doi:10.1002/2017JA024776
905
- 906 King, J. H., and Papitashvili, N. E. (2005). Solar wind spatial scales in and comparisons of
907 hourly Wind and ACE plasma and magnetic field data. *J. Geophys. Res.*, *110*, A02104.
908 doi:10.1029/2004JA010649
909
- 910 Kissinger, J., McPherron, R. L., Hsu, T. -S. and Angelopoulos, V. (2012). Diversion of plasma
911 due to high pressure in the inner magnetosphere during steady magnetospheric convection.
912 *J. Geophys. Res.*, *117*, A05206. doi:10.1029/2012JA017579
913
- 914 Khurana, K. K., Walker, R. J., and Ogino, T. (1996). Magnetospheric convection in the
915 presence of interplanetary magnetic field By: A conceptual model and simulations. *J.*
916 *Geophys. Res.*, *101* (A3), 4907–4916. doi:10.1029/95JA03673
917
- 918 Kubyshkina, D. I., Sormakov, D. A., Sergeev, V. A., Semenov, V. S., Erkaev, N. V., Kubyskin, I.
919 V., Ganushkina, N. Yu. And Dubyagin, S. V. (2014). How to distinguish between kink and
920 sausage modes in flapping oscillations? *J. Geophys. Res.*, *119*, 3,002-3,015.
921 doi:10.1002/2013JA019477.
922
- 923 Laakso, H., C. Perry, S. McCaffrey, D. Herment, A.J. Allen, C.C. Harvey, C.P. Escoubet, C.
924 Gruenberger, M.G.G.T. Taylor, and R. Turner (2010), Cluster Active Archive: Overview, 3-37,
925 The Cluster Active Archive, Astrophysics and Space Science Proceedings, H. Laakso et al.
926 (eds.), Springer.
927
- 928 Lockwood, M. (1993), Modelling high-latitude ionosphere for time-varying plasma
929 convection. IEE Proceedings-H, Vol. 140. No. 2. doi:10.1049/ip-h-2.1993.0015
930
- 931 Malova, H. V., Zelenyi, L. M., Popov, V. Y., Petrukovich, A. A. and Runov, A. V. (2007).
932 Asymmetric thin current sheets in the Earth's magnetotail. *Geophys. Res. Lett.*, *34* (16),
933 L16108. doi:10.1029/2007GL030011
934
- 935 McPherron, R. L., Hsu, T. -S., Kissinger, J., Chu, X., and Angelopoulos, V., (2011).
936 Characteristics of plasma flows at the inner edge of the plasma sheet. *J. Geophys. Res.*, *116*
937 (A5), A00133. doi:10.1029/2010JA015923
938
- 939 Nakamura, R., Baumjohann, W., Klecker, B., Bogdanova, Y., Balogh, A., Rème, H., Bosqued, J.
940 M., Dandouras, I., Sauvaud, J. A., Glassmeier, K. -H., Kistler, L., Mouikis, C., Zhang, T. L.,
941 Eichelberger, H. and Runov, A. (2002). Motion of the dipolarization front during a flow burst
942 event observed by Cluster. *Geophys. Res. Lett.*, *29* (20), 1942. doi:/10.1029/2002GL015763
943
- 944 Nakamura, R., Retinò, A., Baumjohann, W., Volwerk, M., Erkaev, N., Klecker, B., Lucek, E. A.,
945 Dandouras, I., André, M. and Khotyainstev, Y. (2009). Evolution of dipolarization in the near-
946 Earth current sheet induced by Earthward rapid flux transport. *Ann. Geophys.*, *27*, 1743-
947 1754. doi:10.5194/angeo-27-1743-2009
948

- 949 Ness, N. F. (1965). The Earth's Magnetic Tail. *J. Geophys. Res.*, *70* (13), 2989–3005.
950 doi:10.1029/JZ070i013p02989
- 951
- 952 Newell, P. T., Sotirelis, T., Liou, K., Meng, C. -I. and Rich, F. J. (2007). A nearly universal solar
953 wind-magnetosphere coupling function inferred from 10 magnetospheric state variables. *J.*
954 *Geophys. Res.*, *112* (A1), A01206. doi: 10.1029/2006JA012025
- 955
- 956 Nishitani, N., Ruohoniemi, J. M., Lester, M., Baker, J. B. H., Koustov, A. V., Shepherd, S. G.,
957 Chisham, G., Hori, T., Thomas, E. G., Makarevich, R. A., Marchaudon, A., Ponomarenko, P.,
958 Wild, J. A., Milan, S. E., Bristow, W. A., Devlin, J., Miller, E., Greenwald, R. A., Ogawa, T. and
959 Kikiuchi, T. (2019). Review of the accomplishments of mid-latitude Super Dual Auroral Radar
960 Network (SuperDARN) HF radars. *Progress in Earth and Planetary Science*, *6*:27.
961 doi:10.1186/s40645-019-0270-5
- 962
- 963 Ohma, A., Østgaard, N., Reistad, J. P., Tenfjord, P., Laundal, K. M., Moretto Jørgensen, T.,
964 Haaland, S. E., Krcelic, P. and Milan, S. (2019). Observations of Asymmetric Lobe Convection
965 for Weak and Strong Tail Activity. *J. Geophys. Res.: Space Physics*, *124* (12).
966 doi:10.1029/2019JA026773
- 967
- 968 Pettigrew, E. D., Shepherd, S. G. and Ruohoniemi, J. M. (2010). Climatological patterns of
969 high-latitude convection in the Northern and Southern hemispheres: Dipole tilt
970 dependencies and interhemispheric comparisons. *J. Geophys. Res.*, *115*, doi:
971 10.1029/2009JA014956.
- 972
- 973 Petrukovich, A. A. (2011). Origins of plasma sheet B_y . *J. Geophys. Res.*, *116* (A7), A07217.
974 doi:10.1029/2010JA016386
- 975
- 976 Petrukovich, A. A., Baumjohann, W., Nakamura, R., Schödel, R., and Mukai, T. (2001). Are
977 earthward bursty bulk flows convective or field-aligned? *J. Geophys. Res.*, *106* (A10), 21,211-
978 21,215. doi:10.1029/2001JA900019
- 979
- 980 Petrukovich, A. A., Baumjohann, W., Nakamura, R., Runov, A., and Balogh, A. (2005). Cluster
981 vision of the magnetotail current sheet on a macroscale. *J. Geophys. Res.*, *110* (A6), A06204.
982 doi:10.1029/2004JA010825
- 983
- 984 Pitkänen, T., Hamrin, M., Norqvist, P., Karlsson, T., and Nilsson, H. (2013). IMF dependence
985 of the azimuthal direction of earthward magnetotail fast flows. *Geophys. Res. Lett.*, *40* (21),
986 5598-5604. doi:10.1002/2013GL058136
- 987
- 988 Pitkänen, T., Hamrin, M., Norqvist, P., Karlsson, T., Nilsson, H., Kullen, A., Imber, S. M. and
989 Milan, S. E. (2015). Azimuthal velocity shear within an earthward fast flow: further evidence
990 for magnetotail untwisting? *Ann. Geophys.*, *33*, 245-255. doi:10.5194/angeo-33-245-2015
- 991
- 992 Pitkänen, T., Hamrin, M., Karlsson, T., Nilsson, H., and Kullen, A. (2017). On IMF B_y -Induced
993 Dawn-Dusk Asymmetries in Earthward Convective Fast Flows. In: Haaland, S. et al. (2017),
994 *Dawn-Dusk Asymmetries in Planetary Plasma Environments*, John Wiley and Sons, Inc., 107-
995 123.

- 996
 997 Pitkänen, T., Kullen, A., Laundal, K. M., Tenfjord, P., Shi, Q. Q. Park. J. -S., Hamrin, M., De
 998 Spiegeleer, A., Chong, G. S. and Tian, A. M. (2019). IMF B_y Influence on Magnetospheric
 999 Convection in Earth's Magnetotail Plasma Sheet. *Geophys. Res. Lett.*, *46* (21), 11,698-11,708.
 1000 doi:10.1029/2019GL084190
 1001
 1002 Reistad, J. P., Østgaard, N., Tenfjord, P., Laundal, K. M., Snekvik, K., Haaland, S., Milan, S. E.,
 1003 Oksavik, K., Frey, H. U. and Grocott, A. (2016). Dynamic effects of restoring footprint
 1004 symmetry on closed magnetic field lines. *J. Geophys. Res.: Space Physics*, *121* (5),
 1005 015JA022058. doi:10.1002/2015JA022058
 1006
 1007
 1008 Reistad, J. P., Østgaard, N., Laundal, K. M., Ohma, A., Snekvik, K., Tenfjord, P., Grocott, A.,
 1009 Oksavik, K., Milan, S. E. and Haaland, S. (2018). Observations of asymmetries in ionospheric
 1010 return flow during different levels of geomagnetic activity, *J. Geophys. Res.*, *123*.
 1011 doi:10.1029/2017JA025051
 1012
 1013
 1014 Rème, H., Bosqued, J. M., Sauvaud, J. A., Cros, A., Dandouras, J., Aoustin, C., Bouyssou, J.,
 1015 Camus, Th., Cuvilo, J., Martz, C., Médale, J. L., Perrier, H., Romefort, D., Rouzaud, J., d'Uston,
 1016 C., Möbius, E., Crocker, K., Granoff, M., Kistler, L. M., Popecki, M., Hovestadt, D., Klecker, B.,
 1017 Paschmann, G., Scholer, M., Carlson, C. W., Curtis, D. W., Lin, R. P., McFadden, J. P.,
 1018 Formisano, V., Amata, E., Bavassano-Cattaneo, M. B., Baldetti, P., Belluci, G., Bruno, R.,
 1019 Chionchio, G., Di Lellis, A., Shelley, E. G., Ghielmetti, A. G., Lennartsson, W., Korth, A.,
 1020 Rosenbauer, H., Lundin, R., Olsen, S., Parks, G. K., McCarthy, M. and Balsiger, H. (1997). The
 1021 Cluster Ion Spectrometry (CIS) Experiment. *Space Sci. Rev.*, *79*, 303-350. doi:10.1007/978-
 1022 94-011-5666-0_12
 1023
 1024 Rong, Z. J., Barabash, S., Stenberg, G., Futaana, Y., Zhang, T. L., Wan, W. X., Wei, Y. and
 1025 Wang, X. -D. (2015). Technique for diagnosing the flapping motion of magnetotail current
 1026 sheets based on single-point magnetic field analysis. *J. Geophys. Res.: Space Physics*, *120* (5),
 1027 3462-3474. doi:10.1002/2014JA020973
 1028
 1029 Runov, A. Nakamura, R., Baumjohann, W., Zhang, T. L., Volwerk, M., Eichelberger, H. -U. and
 1030 Balogh, A. (2003). Cluster observations of a bifurcated current sheet. *Geophys. Res. Lett.*, *30*
 1031 (2), 1036. doi:10.1029/2002GL016136
 1032
 1033 Runov, A., Angelopoulos, V., Sergeev, V. A., Glassmeier, K. -H., Auster, U., McFadden, J.,
 1034 Larson, D. and Mann, I. (2009). Global properties of magnetotail current sheet flapping:
 1035 THEMIS perspectives. *Ann. Geophys.*, *27*, 319-328. doi:10.5194/angeo-27-319-2009
 1036
 1037 Ruohoniemi, J. M. and Baker, K. B. (1998). Large-scale imaging of high-latitude convection
 1038 with Super Dual Auroral Radar Network HF radar observations. *J. Geophys. Res.*, *103* (A9),
 1039 20,797-20,811. doi:10.1029/98JA01288
 1040

- 1041 Ruohoniemi, J. M. and Greenwald, R. A. (1996). Statistical patterns of high-latitude
1042 convection obtained from Goose Bay HF radar observations. *J. Geophys. Res.*, *101* (A10),
1043 21,743-21,763. doi:10.1029/96JA01584
1044
- 1045 Sergeev, V. A., Angelopoulos, V., Gosling, J. T., Cattell, C. A., and Russell, C. T. (1996).
1046 Detection of localized, plasma-depleted flux tubes or bubbles in the midtail plasma sheet. *J.*
1047 *Geophys. Res.*, *101* (A5), 10,817 – 10,826. doi:10.1029/96JA00460
1048
- 1049 Sonnerup, B. U. Ö, and Cahill Jr, L. J. (1967). Magnetopause structure and attitude from
1050 Explorer 12 observations. *J. Geophys. Res.*, *72* (1), 171-183.
1051 doi:10.1029/JZ072i001p00171
1052
- 1053 Sonnerup, B. U. Ö and Scheible, M. (1998). Minimum and Maximum Variance Analysis. In:
1054 Paschmann, G. and Daly, W. (1998), *Analysis Methods for Multi-Spacecraft Data*, pp 185-
1055 220, ESA Publications Division, Noordwijk, Netherlands.
1056
- 1057 Tenfjord, P., Østgaard, N., Snekvik, K., Laundal, K. M., Reistad, J. P., Haaland, S., and Milan, S.
1058 E. (2015). How the IMF B_y induces a B_y component in the closed magnetosphere and how it
1059 leads to asymmetric currents and convection patterns in the two hemispheres. *J. Geophys.*
1060 *Res.: Space Physics*, *120* (11), 9368-9384. doi:10.1002/2015JA021579
1061
- 1062 Tenfjord, P., Østgaard, N., Strangeway, R., Haaland, S., Snekvik, K., Laundal, K. M., Reistad, J.
1063 P. and Milan, S. E. (2017). Magnetospheric response and reconfiguration times following
1064 IMF B_y reversals. *J. Geophys. Res.: Space Physics*, *122* (1), 417-431.
1065 doi:10.1002/2016JA023018
1066
- 1067 Thomas, E. G. and Shepherd, S. G. (2018). Statistical Patterns of Ionospheric Convection
1068 Derived From Mid-Latitude, High-Latitude and Polar SuperDARN HF Observations. *J.*
1069 *Geophys. Res.: Space Physics*, *123* (4), 3196-3216. doi:10.1002/2018JA025280
1070
- 1071 Tsyganenko, N. A. and Andreeva, V. A. (2015). A forecasting model of the magnetosphere
1072 driven by an optimal solar wind coupling function. *J. Geophys. Res.*, *120* (10), 8401-8425.
1073 doi:10.1002/2015JA021641
1074
- 1075 Volwerk, M., Zhang, T. L., Glassmeier, K. -H., Runov, A., Baumjohann, W., Balogh, A., Rème,
1076 H., Klecker, B. and Carr, C. (2008). Study of waves in the magnetotail region with cluster and
1077 DSP. *Advances in Space Research*, *41* (10), 1593-1597. doi:10.1016/j.asr.2007.04.005.
1078
- 1079 Wei, X. H., Cai, C. L., Cao, J. B., Rème, H., Dandouras, I., and Parks, G. K. (2015). Flapping
1080 motions of the magnetotail current sheet excited by nonadiabatic ions. *Geophys. Res. Lett.*,
1081 *42*, 4731-4735. doi:10.1002/2015GL064459
1082
- 1083 Wei, Y. Y., Huang, S. Y., Rong, Z. J., Yuan, Z. G., Jiang, K., Deng, X. H., Zhou, M., Fu, H. S., Yu,
1084 X. D., Xu, S. B., He, L. H. and Deng, D. (2019). Observations of Short-period Current Sheet
1085 Flapping Events in the Earth's Magnetotail. *The Astrophysical Journal Letters*, *874*, 7pp.
1086 doi:10.3847/2041-8213/ab0f28/pdf.
1087

- 1088 Wu, M., Lu, Q., Volwerk, M., Vörös, Z., Ma, X., and Wang, S. (2016). Current sheet flapping
1089 motions in the tailward flow of magnetic reconnection. *J. Geophys. Res.*, *121* (8), 7817-7827.
1090 doi:10.1002/2016JA022819
1091
- 1092 Zhang, L. Q., Baumjohann, W., Wang, C., Dai, L., and Tang, B. B. (2016). Bursty bulk flows at
1093 different magnetospheric activity levels: Dependence of IMF conditions. *J. Geophys. Res.*,
1094 *121* (9), 8773-8789. doi:10.1002/2016JA022397
1095
1096